nature communications

Article

https://doi.org/10.1038/s41467-025-65705-z

Autocrine ECM molecules establish MSC quiescence during incisor development by disrupting WNT ligand trafficking process

Received: 5 April 2025

Accepted: 22 October 2025

Published online: 27 November 2025

Check for updates

Zexi Chen[1,2,6], Meilian Cai[2,3,6], Yuling Wang[2], Xuan Li[4], Yongwen He[5], Hongji Pu[5], Juan Huang[2], Ling Ye[4], Ruili Yang[3] ✉, Junjun Jing[4] ✉ & Hu Zhao[2] ✉

Stem cells support homeostasis and injury repair of adult organs. It remains unclear when and how adult stem cells form during development. Here, we discover that incisor mesenchymal stem cells, marked by an extracellular matrix molecule *Smoc2*, establish their identity and quiescence between E14.5 and E16.5, and persist into adulthood. They support both embryonic tooth development and postnatal organ turnover. Concurrently, the incisor mesenchyme evolves from a homogenous dental papilla into a heterogeneous dental pulp consisting of a complete lineage hierarchy, which persists into adulthood. *Smoc2* and its homologous molecule *Smoc1* are indispensable for maintaining the quiescence and hierarchy of mesenchymal stem cells. They function by disrupting the binding between canonical WNT ligands and glypican, a process critical for transporting hydrophobic WNT ligands within the aqueous niche. In conclusion, mesenchymal stem cells establish their quiescence during development through autocrine extracellular matrix molecules to keep canonical WNT ligands from accessing them.

Developmental biology studies the process through which a single fertilized egg evolves into a complex, multicellular organism, mostly involving prenatal stages. In contrast, stem cell biology investigates how adult stem cells support the self-renewal and regeneration of adult organs and tissues during physiological, injury, and disease conditions. A significant knowledge gap between the two fields is about when and how adult stem cells form during development. Despite research conducted on hematopoietic stem cells, neural stem cells, hair follicle and intestinal stem cells[1–6], the developmental origin and regulatory mechanisms controlling the stem cell emergence in most organs remain largely unknown. Some fundamental questions remain unanswered: Do adult stem cells form by maintaining their embryonic state or through induction? How are tissue stem cells specified to the right place and time? Furthermore, it is unclear whether a common stem/progenitor cell population supports organ formation during both development and adulthood[7,8].

Mesenchymal stem cells (MSCs) are a type of multipotent stem cell that can differentiate into a variety of cell types and have been found in various tissues, including bone marrow, adipose tissue, long bone, and teeth[9–14]. During development, MSCs can originate from either neural crest cells or mesoderm, depending on whether they are located in the craniofacial or trunk region[15–18]. The mechanisms underlying the formation of MSCs during development, including when and how they form, have not yet been fully elucidated.

The major challenge lies in the lack of molecular markers to label stem cells during the embryonic stage. Lineage tracing experiments

[1]Academy for Advanced Interdisciplinary Studies, Peking University, Beijing, China. [2]Chinese Institute for Brain Research, Beijing, China. [3]Department of Orthodontics, Peking University School and Hospital of Stomatology, National Center for Stomatology & National Clinical Research Center for Oral Diseases & National Engineering Research Center of Oral Biomaterials and Digital Medical Devices, Beijing, China. [4]State Key Laboratory of Oral Diseases, National Center for Stomatology, National Clinical Research Center for Oral Diseases, West China Hospital of Stomatology, Sichuan University, Chengdu, China. [5]Qujing Medical College, Qujing City, Yunnan Province, China. [6]These authors contributed equally: Zexi Chen, Meilian Cai. ✉e-mail: ruiliyang@bjmu.edu.cn; junjunjing@scu.edu.cn; zhaohu@cibr.ac.cn

based on transgenic models have become the gold standard for studying adult stem cells in adult tissues and organs. However, most of the molecular markers used to label adult stem cells lose their specificity during embryonic stages, making it difficult to map the lineage fate of potential embryonic stem cell populations.

The mouse incisor occupies nearly the entire mandible and is a classical model for both developmental and stem cell biology[19,20]. During adulthood, mouse incisors undergo rapid turnover supported by epithelial stem cells within the cervical loop and MSCs located surrounding this region[21–23]. Incisor MSCs are located at the apical region surrounding the neurovascular bundle (NVB), under the influence of niche signaling cues (Fig. 1a)[23]. Inside the pulp, these MSCs generate transit-amplifying cells (TA cells) positioned beneath them. TA cells subsequently differentiate into distal pulp fibroblasts and odontoblasts, which secrete matrix to form calcified dentin. Outside the pulp, incisors are encapsulated by dental follicle tissue composed of periodontal ligament and supporting alveolar bone (Fig. 1a)[24]. The finely organized differentiation hierarchy, together with the rapid turnover rate property of the incisor, makes it an ideal model for stem cell research (Fig. 1a)[25–29].

Here, we identified an extracellular matrix (ECM) molecule *Smoc2* (SPARC-related modular calcium-binding protein2), as an MSC marker for both adult and embryonic incisors[30]. *Smoc2*+ cells population supports both the developmental process and adult incisor turnover. Instead of maintaining an embryonic status of active proliferation, the *Smoc2*+ cells acquire quiescence between E14.5 and E16.5. *Smoc2*, together with *Smoc1*, is indispensable for establishing quiescence and hierarchy by inhibiting canonical *Wnt* activity. As ECM proteins, *Smoc1/2* inhibit *Wnt* activity by regulating the WNT ligand trafficking process and preventing WNT ligands from accessing stem cells, thereby establishing and maintaining MSCs quiescence. Our study provides a mechanism to explain when and how MSCs form during development.

Results

Smoc2+ cells are mesenchymal stem cells for adult mouse incisor pulp

To identify new markers for studying MSC development, we first performed single-cell RNA sequencing (scRNA-seq) on adult mouse incisors. Following similar landmark genes from previous research, incisor mesenchyme can be clustered into five groups, including apical pulp (MSCs region), mitotic pulp (TA cells region), distal pulp, odontoblasts, and dental follicle (Fig. 1b)[24]. UMAP revealed that the *Smoc2* (SPARC-related modular calcium-binding protein 2) gene is highly enriched in the apical pulp cluster, which is consistent with a previous study[24]. Pseudotime and velocity analysis also suggested that *Smoc2* marks a primitive population (Fig. 1c, d).

To validate the expression of *Smoc2* in the incisor mesenchyme, we performed RNAscope analysis and found that *Smoc2* is specifically expressed at the apical mesenchyme of adult mouse incisor, but not in periodontal mesenchyme or dental epithelium (Fig. 1f). Moreover, *Smoc2-mScarlet* reporter strain was generated, which demonstrated a consistent expression pattern as RNAscope (Fig. 1g). Immunostaining with β3-tubulin and αSMA antibodies showed *Smoc2*+ cells surrounding the proximal region of the neurovascular bundle (NVB) (Supplementary Fig. 1a, b). Immunostaining of Ki67, Sp7, or Col1 antibodies suggested that *Smoc2*+ cells in adult incisors are quiescent and undifferentiated (Fig. 1h–j). To determine the dynamic property of *Smoc2*+ cells, *Smoc2-mScarlet* mice were injected with EdU and BrdU to perform co-localization analysis of *Smoc2*+ cells and label-retaining cells (LRCs) (Supplementary Fig. 1c–g)[31,32]. We found that LRCs exhibited no overlap with BrdU-positive cells, which marked fast-cycling populations, indicating distinct cellular states between LRCs and fast-cycling cells (Supplementary Fig. 1d–e). Quantitative analysis revealed that approximately 85% of *Smoc2-mScarlet*+ cells were identified as LRCs, while 95% of LRCs were found to be *Smoc2*+ (Supplementary Fig. 1f, g). These data demonstrated that *Smoc2*+ cells are slow-cycling LRCs.

To demonstrate whether *Smoc2*+ cells are a stem cell population, we generated *Smoc2-CreERT2;Ai14* mice to perform lineage tracing experiment. We injected tamoxifen at postnatal day 56 (P56) of age (Fig. 1k), and we found that *Smoc2*+ cells specifically reside in the proximal region of the incisor mesenchyme 24 hours after induction, consistent with RNAscope analysis. (Fig. 1l). *Smoc2*+ cells start to contribute to the pulp and odontoblast lineages four weeks after induction (Fig. 1m, n). Most of pulp cells (~85%), odontoblasts (~66%), and part of PDL (~13%) were labeled one year after induction, indicating *Smoc2*+ cells are indeed MSCs for the incisor mesenchyme (Fig. 1o, p). Interestingly, the central pulp mesenchyme, possibly the neurovascular bundle, is located, remained largely unlabeled. No contribution towards alveolar bone was detected (Fig. 1o", r). Lineage tracing contribution time courses are similar in both upper and lower incisors (Fig. 1q).

Gli1 is the most commonly used MSC marker for incisor and other mesenchymal tissue[23,33]. Sequencing analysis revealed that both *Gli1*+ and *Smoc2*+ cells are located within similar mesenchymal compartments, although *Gli1*+ cells are in a broader area. (Supplementary Fig. 1h). To compare these two populations, we generated *Smoc2-mScarlet;Gli1-GFP* and found that 98.53% of *Smoc2*+ cells were *Gli1*+, whereas 59% of *Gli1*+ cells were *Smoc2* + (Supplementary Fig. 1i, j), suggesting that Smoc2+ cells are a portion of Gli1+ cells in the incisor. Moreover, lineage tracing analysis showed that *Gli1* + cells contribute to over 90% of the incisor pulp, and periodontal mesenchyme within 4 weeks after induction. In contrast, *Smoc2*+ cells require one year to contribute to majority of the pulp (Supplementary Fig. 1k–m). These data suggest *Gli1*+ cells may contain another stem cell population with higher turnover rate and more differentiation capability.

To examine whether *Smoc2*+ cells are able to respond to injury repair, we performed a needle injury assay for lower incisor in *Smoc2-CerERT2; Ai14* mice (Supplementary Fig. 1n). EdU assay indicated that *Smoc2*+ cells are more actively proliferating in the injury side than that of the control side (Supplementary Fig. 1o–q), indicating *Smoc2*+ cells are responsive to injury repair.

Collectively, *Smoc2*+ cells as quiescent stem cells contributing to incisor pulp fibroblast, odontoblast and periodontal mesenchyme of adult incisor. In addition, the *Smoc2*+ lineage was also observed to contribute to perivascular cells and to the postnatal condylar process (data not shown), indicating their diverse lineage potential. They are a subset of *Gli1* + MSCs and can be activated by injury.

Smoc2+ cells are stem cells for E16.5 incisor mesenchyme

E16.5 marks the bell stage in incisor development and is considered the point at which all lineages initially form[19]. We performed scRNA-seq on the incisor mesenchyme of E16.5 mouse embryos. Based on differential gene expression analysis, the E16.5 incisor mesenchyme could be clustered into similar compartments as in adult incisors. Interestingly, *Smoc2* was again highlighted in the apical pulp, the presumable stem cell population (Fig. 2a). UMAP, pseudotime and velocity analysis suggested that *Smoc2*+ cells are the most primitive population for E16.5 dental mesenchyme (Fig. 2b–d).

Next, we verified *Smoc2* expression using RNAscope on embryos at different stages. At E12.5 (bud stage) or E13.5 (cap stage), no signal was detected in the incisor tooth germs (Fig. 2e, f). At E14.5 (cap stage), *Smoc2* mRNA was detectable in the proximal region of the tooth germ (Fig. 2g). At both E16.5 and E18.5 (bell stage), *Smoc2* expression is specifically expressed in the presumable stem cell region, similar to that in adult incisors (Fig. 2h, i). Co-staining with Ki67 and Sp7 antibodies showed that *Smoc2*+ cells in E16.5 embryos are mostly negative of Ki67 and all negative for Sp7, indicating that they are quiescent and undifferentiated (Fig. 2j, k).

https://doi.org/10.1038/s41467-025-65705-z

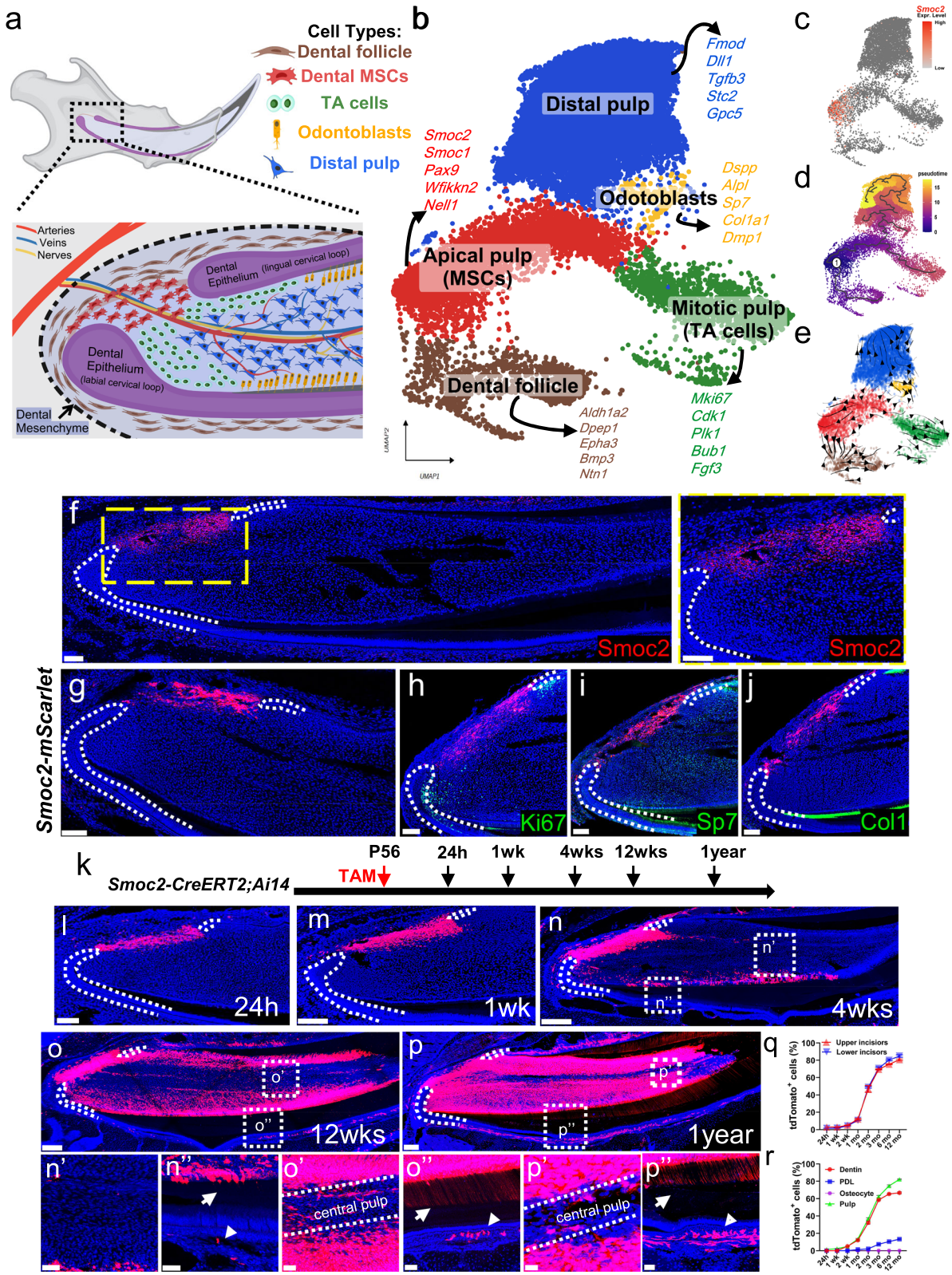

To confirm that *Smoc2*+ cells are stem cells at E16.5, we performed lineage tracing analysis in *Smoc2-CerERT2;Ai14* mice indued with tamoxifen at E16. We found that *Smoc2*+ cells were present in the apical pulp mesenchyme 12 hours after induction (Fig. 2l, m). The results collected at P1, P7 and P21 clearly showed that *Smoc2*+ cells gradually contributed to the incisor mesenchyme to support both development and homeostasis of incisor mesenchyme (Fig. 2o, p). At P56, nearly 80% of pulp mesenchyme and odontoblasts, approximately 90% of periodontal mesenchyme, and approximately 5% of alveolar bone osteocytes were derived from *Smoc2*+ cells (Fig. 2q, r). Interestingly, the central pulp mesenchyme in both P21 and P56 samples remained largely unlabeled (Fig. 2p', q'').

Smoc2+ cell clones lineage tracing was performed in *Smoc2-CerERT2; Ai14* mice induced by a low dosage of tamoxifen at E16

Fig. 1 | *Smoc2*+ cells are mesenchymal stem cells for adult mouse incisor mesenchyme. a A schematic drawing illustrates the mesenchymal cell populations within an adult mouse incisor. Created with MedPeer (medpeer.cn). **b** UMAP plot with annotations. **c** Feature plot of *Smoc2*, **d** Monocle analysis and **e** Velocity analysis of adult mouse incisor mesenchyme. RNAscope staining of *Smoc2* in the adult mouse incisor. The dotted box in the apical pulp region (**f**) is enlarged on right. Scale bars: 100 μm. Representative images from three independent experiments with similar results. **g**–**j** *Smoc2*+ cells in the incisor mesenchyme of the *Smoc2-mScarlet* reporter mouse. Co-localization analysis of *Smoc2*+ cells with Ki67+ cells (**h**), Sp7+ cells (**i**), and Col1+ cells (**j**) in the incisor mesenchyme of the *Smoc2-mScarlet* reporter mouse. Scale bars: 100 μm. Representative images from three independent experiments with similar results. Lineage tracing analysis for adult *Smoc2-CreERT2;Ai14* mouse incisors. (**k**) Injection protocol of the lineage tracing experiment. **l**–**p** Lineage tracing analysis was performed on adult *Smoc2-CreER-T2;Ai14* mice incisor. The dotted boxes in (**n**–**p**) are enlarged in (**n'-p"**), respectively. Scale bars: 200 μm in **l**–**p** and 50 μm in **n'**–**p"**. Representative images from three independent experiments with similar results. **q** Quantitative analysis of the contribution of *Smoc2*+ cells to mesenchymal lineages within the upper and lower incisor at various time points, calculated from sections obtained in experiments of the same type as shown in (**l**–**p**). Data are presented as mean ± SEM. $n = 3$ biological replicates. **r** Quantitative analysis of the contribution of *Smoc2*+ cells to different incisor mesenchymal compartments at various time points, calculated from sections obtained in experiments of the same type as shown in (**l**–**p**). Data are presented as mean ± SEM. $n = 3$ biological replicates. White dotted lines in (**f**–**p**) outline incisor cervical loops epithelium. Source data are provided as a Source Data file.

(Supplementary Fig. 2a, b). We found that sporadically labeled *Smoc2*+ cells are able to give rise to different clones in pulp mesenchyme, odontoblasts, and periodontal mesenchyme, indicating their multipotential differentiation capability (Supplementary Fig. 2c).

Next, tri-lineage differentiation assays were performed. *Smoc2*+ cells isolated from *Smoc2-mScarlet* mice using flow cytometry at E16.5 possess tri-lineage differentiation capacity (Supplementary Fig. 2d). Clonal culture assays were performed using cells isolated from *Smoc2-CerERT2; Ai14* mice induced at E16. The tdTomato+ clones were able to expand into large clones in 21 days (Supplementary Fig. 2e). These experiments showed that *Smoc2*+ cells at E16.5 exhibit typical MSC characteristics in vitro.

To systematically dissect the transcriptional dynamics of *Smoc2*+ cells across development, we first employed a Venn diagram analysis to compare the top 5000 expressed genes between E16.5 and P56 stages, revealing 4199 commonly shared genes and 801 stage-specific genes (Supplementary Fig. 3a). To investigate functional differences, we analyzed the signaling pathways and biological processes associated with these subsets (Supplementary Fig. 3b–d). At E16.5, these cells were enriched for pathways related to anatomical structure development, regulation of vasculature development, and myeloid cell development, highlighting their role in early tissue patterning (Supplementary Fig. 3b). In contrast, adult Smoc2+ cells exhibited strong associations with immune response and endothelial barrier establishment, reflecting their adapted functions in postnatal tissue maintenance (Supplementary Fig. 3d). Differential expression analysis identified 71 upregulated and 28 downregulated genes in adult *Smoc2*+ cells relative to E16.5 (Supplementary Fig. 3e). Downregulated genes in adults were linked to extracellular structure organization, mesenchyme development, and Wnt signaling (Supplementary Fig. 3f). Genes without significant differential expression were enriched for processes such as protein localization regulation, mRNA processing, histone modification, and autophagy (Supplementary Fig. 3g). Upregulated genes were tied to BMP signaling, osteoblast differentiation, and interferon response (Supplementary Fig. 3h). This analysis underscores the dynamic yet conserved molecular identity of *Smoc2*+ cells across postnatal life, balancing quiescence-associated functions with stage-specific adaptations.

Therefore, *Smoc2*+ cells at E16.5 are MSCs for the incisor pulp and contribute to both embryonic development and postnatal turnover. They share a highly similar transcription profile with that of adult MSCs.

Incisor mesenchyme hierarchy is established between E14.5-E16.5

Most tissues and organs comprise cells at various differentiation stages along a lineage trajectory, from stem cells to terminally differentiated cells[34–36]. To analyze the developmental processes and hierarchical formation of the incisor mesenchyme, we performed scRNA-seq on incisor mesenchyme at different developmental stages, including E13.5, E14.5, E15.5, E16.5, E18.5, and P56 (Supplementary Fig. 4a, b).

UMAP and heatmap analyses revealed a similar developmental trajectory for the incisor mesenchyme (Fig. 3a, b). At E13.5, two primary clusters were present: the dental papilla and the dental follicle. By E14.5, the dental papilla segregated into a relatively quiescent apical pulp population and an actively dividing mitotic pulp cluster. At E16.5, odontoblast and distal pulp populations emerged, establishing a five-compartment hierarchy (dental follicle, apical pulp, mitotic pulp, distal pulp, and odontoblasts) that persisted into adulthood. While the E18.5 profile resembled E16.5, the distal pulp population expanded significantly within the pulp, a trend that continued into adulthood.

To validate the sequencing results, we performed MiP-Seq for key hierarchical genes in developing incisors at different stages (Fig. 3c–w, Supplementary Figs. 5–9)[37]. We found that all dental follicle markers appeared at E14.5 outside of the dental pulp and maintained the similar pattern into adulthood (Fig. 3c–f, Supplementary Fig. 5). Some apical pulp marker genes (*Smoc1*, *Smoc2*, and *Pax9*) appeared at E14.5 in the apical region, while others (*Wfikkn2* and *Nell1*) appeared at E16.5 in the apical region (Fig. 3g–j, Supplementary Fig. 6). All apical pulp markers maintained their apical expression pattern into adulthood. Mitotic pulp markers were detected throughout the majority of the dental mesenchyme at E14.5 but became restricted to the cervical loop region from E16.5 onwards (Fig. 3k–n, Supplementary Fig. 7). Moreover, distal pulp and odontoblast clusters suggest that these two cell populations are formed at E16.5 (Fig. 3o–w, Supplementary Fig. 8, 9). Thus, the incisor mesenchyme progressively establishes its lineage hierarchy between E14.5 and E16.5, transitioning from a relatively homogeneous population to a well-organized structure comprising the aforementioned hierarchical organization that persists into adulthood.

Quiescence of *Smoc2*+ mesenchymal stem cells is established between E14.5 and E16.5

Quiescence is a state of prolonged and reversible cell cycle exit, distinct from the irreversible cell-cycle exit that characterizes terminal cell differentiation or senescence[38].

At E13.5, a violin plot of the sequencing data showed that the dental papilla highly expressed proliferation-related markers (*MKi67, Cdk1, Bub1, Plk1*, and *Top2a*), indicating that they are highly proliferative. At E14.5, the dental papilla population segregated into *Smoc2*+ apical pulp with low expression levels of proliferation markers, and the mitotic pulp with high expression levels of proliferation markers. At E15.5, E16.5, E18.5, and P56, the *Smoc2*+ apical pulp population maintained low expression, while the mitotic pulp continued to exhibit high expression of these proliferation markers (Fig. 4a).

Next, we performed Ki67 staining on incisor tooth germs from *Smoc2-mScarlet* mice. At E14.5, approximately 36% of *Smoc2*+ cells were Ki67 + . The proportion of Ki67+;*Smoc2*+ cells decreased to 3.8% at E16.5 and remained at a low level at both E18.5 (3.3%) and P56 (2.6%)

https://doi.org/10.1038/s41467-025-65705-z

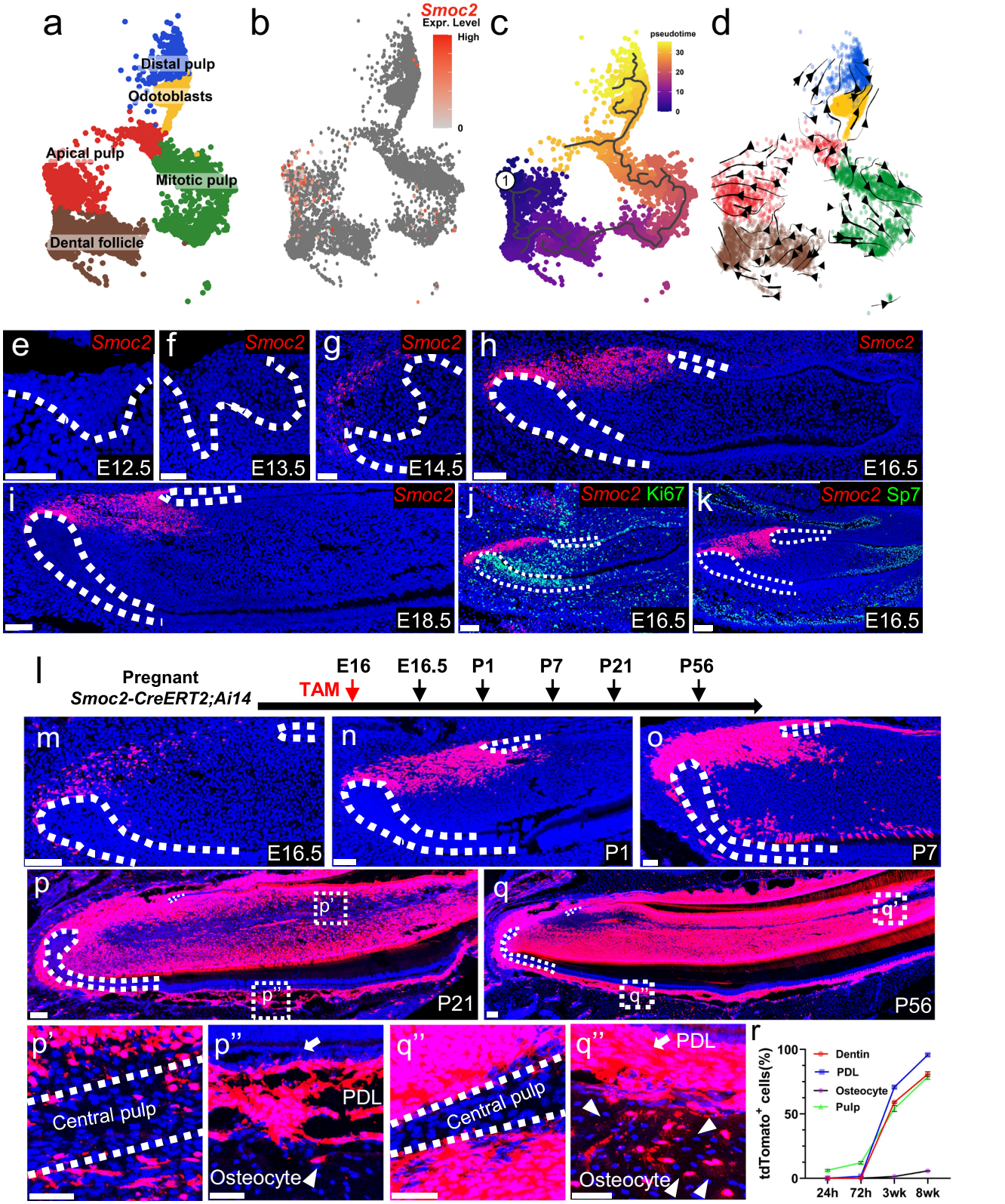

Fig. 2 | *Smoc2*+ cells are mesenchymal stem cells of mouse incisor mesenchyme at E16.5. a UMAP plot with annotations, **b** Feature plot of *Smoc2*, **c** Monocle analysis and **d** Velocity analysis of incisor mesenchyme at E16.5. **e**–**k** RNAscope staining of *Smoc2* in WT incisors at different embryonic stages. Co-localization analysis of *Smoc2* with Ki67 (**j**) and Sp7 (**k**) in the WT incisor at E16.5. White dotted lines outline incisor dental epithelium. Representative images from three independent experiments with similar results. Scale bars: 50 μm. **l**–**q** Lineage tracing analysis for mouse incisor at E16.5. **l** The tamoxifen induction protocol of lineage tracing experiments. **m**–**q** Lineage tracing analysis of *Smoc2*+ cells in the incisor mesenchyme at various time points after induction. White dotted lines outline cervical loop epithelium. White dotted boxes in (**p**, **q**) are enlarged (**p′**, **q″**). Scale bars: 100 μm in (**m**–**q**) and 50μm in (**p′**, **q″**). Representative images from three independent experiments with similar results. **r** Quantitative analysis of the contribution of *Smoc2*+ cells to different incisor mesenchymal compartments at various time points, calculated from sections obtained in experiments of the same type as shown in (**m**–**q**). Data are presented as mean ± SEM. *n* = 3 biological replicates. Source data are provided as a Source Data file.

https://doi.org/10.1038/s41467-025-65705-z

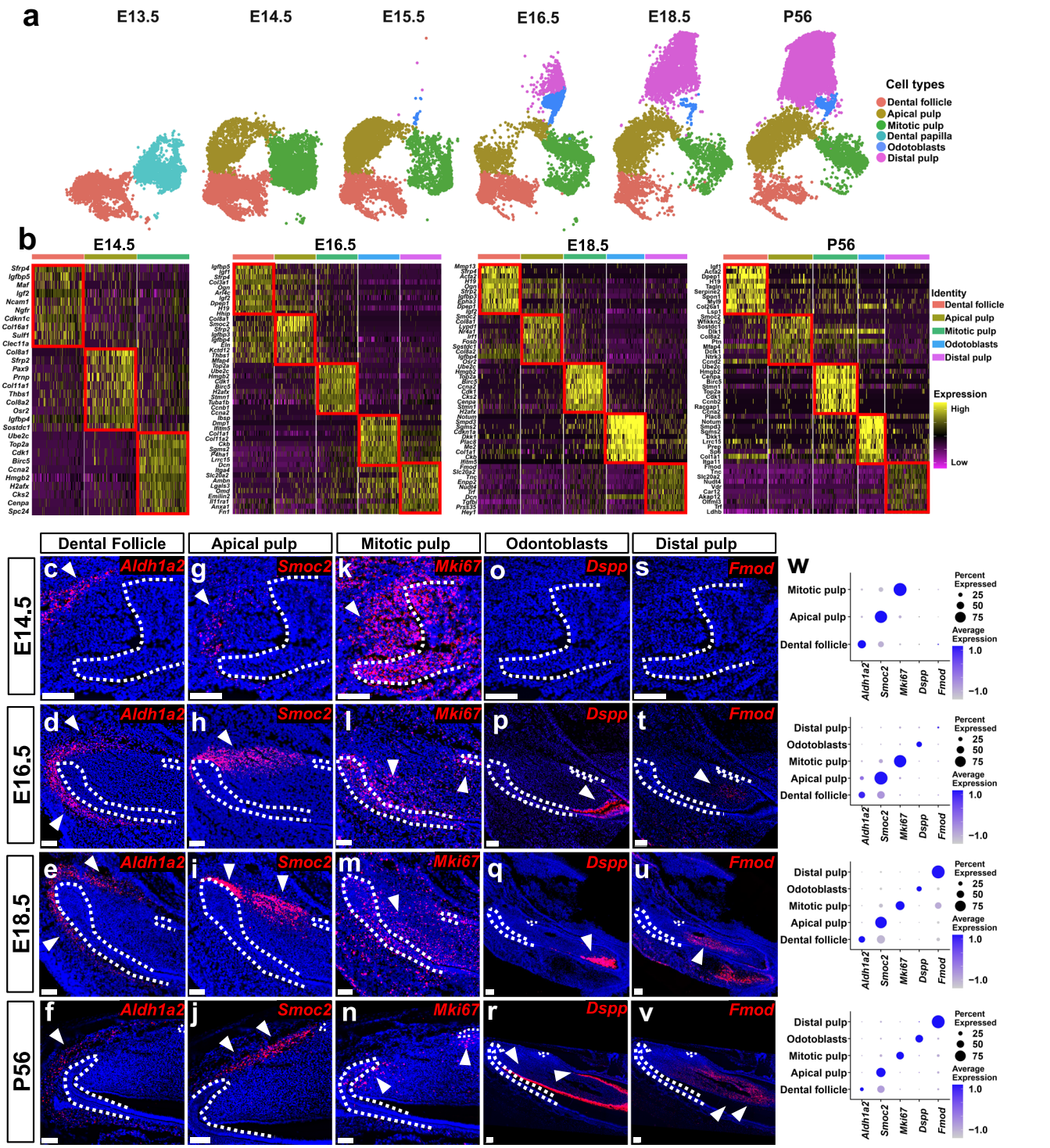

Fig. 3 | The lineage hierarchy of incisor mesenchyme is established between E14.5 and E16.5. a UMAP plots of the incisor mesenchyme at E13.5, E14.5, E15.5, E16.5, E18.5 and P56. **b** Heatmap of signature genes in the incisor mesenchyme at E14.5, E16.5, E18.5, and P56. **c**–**v** Mip-seq analysis of signature genes in the incisor mesenchyme at E14.5, E16.5, E18.5, and P56. White arrows indicate regions with signals. White dotted lines outline the dental epithelium. Scale bars: 100 μm. Representative images from three independent experiments with similar results. **w** Dotplot visualizing representative genes in each cell cluster of incisor mesenchyme at E14.5, E16.5, E18.5, and P56.

(Fig. 4b, c). The number of *Smoc2*+ cells in each incisor was less than 100 per incisor at E14.5 and rapidly increased to over 300 per incisor at E16.5. The number of *Smoc2*+ cells remained at approximately 400 per incisor at both E18.5 and adult stages (Fig. 4d). In contrast, the proportion of *Smoc2*+ cells within each incisor continuously decreased from 14% at E14.5 to 1.1% at P56 (approximately 14% at E14.5, 11% at E16.5, 8.7% at E18.5, and 1.1% at P56) (Fig. 4e).

Therefore, *Smoc2*+ incisor MSCs acquire their quiescence and quantity between E14.5 and E16.5 and maintain these characteristics into adulthood.

Smoc1/2 loss depletes the stem cell pool and quiescence

Next, we sought to identify functions of *Smoc2* during incisor development. *Smoc2* is an ECM protein of the SPARC/osteonectin family[30,39].

https://doi.org/10.1038/s41467-025-65705-z

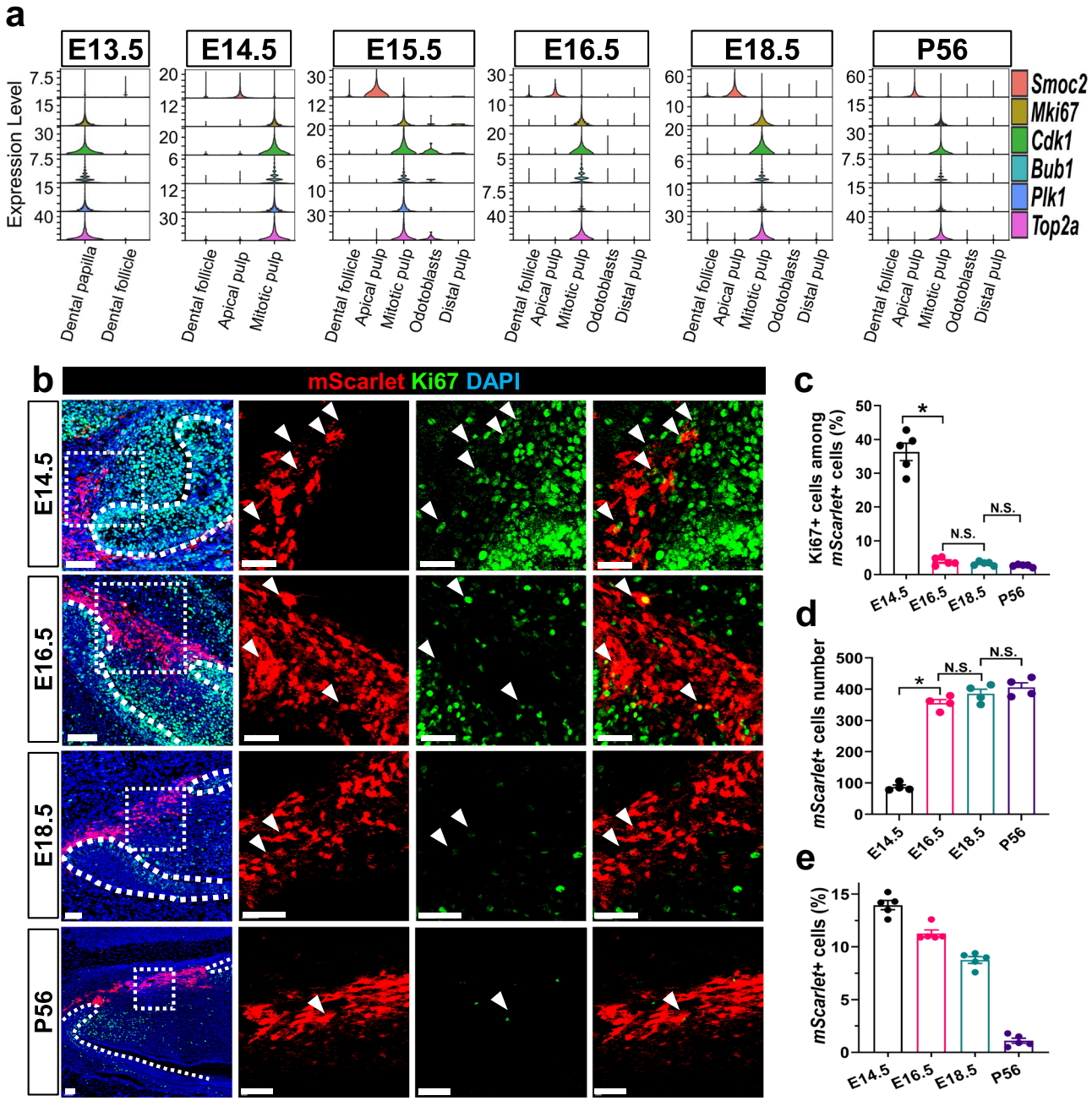

Fig. 4 | The quiescence of incisor mesenchymal stem cells is established between E14.5 and E16.5. a Violin plot visualizing expression levels of *Smoc2* and proliferation-related genes in the dental mesenchyme of incisors at E13.5, E14.5, E15.5, E16.5, E18.5 and P56. **b** Co-localization analysis of *Smoc2*+ cells and Ki67+ cells in the incisor mesenchyme of *Smoc2-mScarlet* mice at E14.5, E16.5, E18.5, and P56. Boxed regions were enlarged and displayed in the right panels. White dotted lines outline the dental epithelium. White arrows point to Ki67+ cells among *mScarlet*+ cells. Scale bars: 50 μm. Representative images from three independent experiments with similar results. **c** Quantitative analysis of the percentage of Ki67+ cells among *mScarlet*+ cells, calculated from sections obtained in experiments of the same type as shown in (**b**). Data are presented as mean ± SEM. $n = 3$ biological replicates; unpaired two-tailed Student's *t*-test. E14.5 vs E16.5, $p = 9.0 \times 10^{-6}$; E16.5 vs E18.5, $p = 0.3037$; E18.5 vs P56, $p = 0.0869$; N.S.: not significant. **d** Quantitative analysis of the number *Smoc2-mScarlet*+ cells within incisor pulp at various time points, calculated from sections obtained in experiments of the same type as shown in (**b**). Data represent mean ± SEM. $n = 4$ biological replicates; unpaired two-tailed Student's *t*-test. E14.5 vs E16.5, $p = 1.3 \times 10^{-6}$; E16.5 vs E18.5 $p = 0.1474$; E18.5 vs P56, $p = 0.3619$; N.S.: not significant. **e** Quantitative analysis of the percentage of *Smoc2-mScarlet*+ cells in incisor pulp at various time points, calculated from sections obtained in experiments of the same type as shown in (**b**). Data represent mean ± SEM. $n = 5$ biological replicates. Source data are provided as a Source Data file.

Smoc1, a homolog of *Smoc2*, was identified together with *Smoc2* by sequencing analysis as a potential MSC marker. RNAscope analysis showed specific *Smoc1* expression was detected in the apical pulp region and highly co-localized with *Smoc2* at E14.5 and E16.5 (Supplementary Fig. 10a–d). At E18.5, reduced *Smoc1* expression was detected with a slightly different pattern compared to that at E16.5 (Supplementary Fig. 10e). In adult incisors, weak *Smoc1* expression was only detected near the apical mesenchyme immediately surrounding the labial and lingual cervical loops (Supplementary Fig. 10f). *Smoc1-/-* mice were generated and the pups died at birth. Ki67 staining showed increased dividing cells in the apical mesenchyme of E18.5 *Smoc1-/-* or *Smoc2-/-* incisors compared to control incisors (Supplementary

Fig. 10g–j). Sp7 staining showed no difference between control and *Smoc1-/-* or *Smoc2-/-* incisors (Supplementary Fig. 10k–n).

Next, we generated *Smoc1-/-; Smoc2-/-* double knockout (*Smoc1/2* DKO) mice. At E13.5, the incisor tooth germs of *Smoc1/2* DKO mice showed no morphological difference compared to the wild-type controls (Supplementary Fig. 11a, d). Ki67 and Sp7 staining signals were also similar to those of the control samples (Fig. 5a, b, g, h). At E14.5, the *Smoc1/2* DKO incisor germs appeared larger than those of the wild-type controls (Supplementary Fig. 11b, e). Dramatically increased Ki67 staining signals was observed in the mutant incisor germs (Fig. 5c, d). Surprisingly, a strong Sp7 staining signal was detected in the mesenchyme of the mutant incisor germs (Fig. 5i, j). At E16.5, the size of the *Smoc1/2* DKO incisor germs was only half of the control samples (Supplementary Fig. 11c, f). Ki67 and Sp7 staining signals were dramatically increased and expanded to the apical region of the mutant incisor embryos at E14.5 and E16.5 (Fig. 5e, f, k, l, Supplementary Fig. 11g, h). Additionally, the size of the cervical loop epithelium reduced in the mutant incisor germs, with increased Ki67 staining signals at E14.5 and E16.5 (Supplementary Fig. 11c, f, i). *Smoc1/2* DKO mice embryos died at birth with severe craniofacial phenotypes, including calvarial bones defects and micrognathia (Fig. 5m, n)[40].

ScRNA-seq was performed for the incisor mesenchyme of E16.5 control and *Smoc1/2* DKO mice. Integrated UMAP and heatmap analysis revealed dramatically different clustering profiles of mesenchymal cells in mutant incisors (Fig. 5o–q). In the *Smoc1/2* DKO mesenchyme, proportions of the apical pulp and distal pulp populations were both dramatically reduced, whereas the mitotic pulp, odontoblast, and dental follicle clusters increased in proportion (Fig. 5p, r).

Integrated UMAP analysis also showed expression of apical pulp marker genes (*Pax9, Gli1*, and *Wifikkn2*) and distal pulp marker genes (*Fmod, Dll1*, and *Stc2*) nearly diminished in the *Smoc1/2* DKO mutant incisor (Fig. 5s, Supplementary Fig. 11 m). Expression of mitotic pulp (*Ki67, Cdk1, Plk1*, and *Bub1*) and odontoblast marker (*Sp7, Alpl, Col1a1*, and *Dmp1*) dramatically increased in the mutant incisor (Supplementary Fig. 11k, l). Expression of dental follicle marker genes (*Dpep1, Bmp3*, and *Epha3*) appeared to reduce in expression level, but expand in distribution range (Supplementary Fig. 11j). Violin plots of K*i67* and *Sp7* furtherly showed increased proliferation and differentiation in the *Smoc1/2 DKO* incisor mesenchyme (Fig. 5t, u). MIP-Seq analysis showed expression of *Ki67, Sp7* was expanded to the apical regions of the mutant incisor mesenchyme (Fig. 5v).

To investigate cell cycle dynamics in control and *Smoc1/2* DKO incisors, we performed dual nucleotide analog labeling using EdU and BrdU[31] (Supplementary Fig. 12a). In control incisors, apical pulp mesenchymal cells exhibited minimal EdU and BrdU incorporation, indicative of a quiescent state (Supplementary Fig. 12b, c). In contrast, *Smoc1/2* DKO incisors displayed a significant increase in the proportion of EdU+ and BrdU+ cells within the apical pulp mesenchyme, demonstrating active DNA synthesis and cell division (Supplementary Fig. 12d–f). Notably, the elevated double positivity for EdU/BrdU in DKO incisors directly reflects a loss of quiescence in response to *Smoc1/2* deficiency. These findings provide critical evidence that *Smoc1/2* is essential for maintaining stem cell quiescence in the incisor apical niche.

To investigate the role of *Smoc1/2* in postnatal development, we generated *Gli1-CreERT2; Smoc1$^{flox/flox}$; Smoc2$^{flox/flox}$; Ai14* (*Smoc1/2* ICKO) mice induced at postnatal days (Supplementary Fig. 12g). Mandibles were harvested at 3 weeks post-induction. *Smoc1/2* ICKO mice were viable but displayed significant morphological abnormalities, including reduced mandible size and shortened incisors compared to control littermates (Supplementary Fig. 12h–k). Notably, quiescence in the apical pulp of *Smoc1/2* ICKO incisors was disrupted, evidenced by increased Ki67+ and EdU+ cell populations (Supplementary Fig. 12l–q). These results indicate that *Smoc1/2* also plays critical roles in maintaining MSC quiescence during postnatal incisor development.

Therefore, *Smoc2*, together with its homolog *Smoc1*, are indispensable for incisor stem cell quiescence, maintenance and mesenchymal hierarchy organization.

Wnt inhibition maintains Smoc2+ mesenchymal stem cell quiescence

To identify the mechanisms through which *Smoc1/2* regulate MSC quiescence, we conducted gene ontology (GO) analysis on scRNA-seq data of *Smoc1/2* DKO incisor mesenchyme. This analysis revealed disruptions in several biological processes, including cell proliferation, ossification, and migration. Notably, aberrations in the Wnt signaling pathway were highlighted as a highly related pathway (Fig. 6a).

Therefore, we evaluated the levels of canonical Wnt activity within *Smoc2* + MSCs. Sequencing analysis showed that, throughout the entire developmental course of incisor mesenchyme, the majority of *Smoc2* + MSCs have low expression levels of *Axin2, Lef1*, *Apc*, *Ccnd1* and *Dvl1*, several indicators of canonical *Wnt* activity (Supplementary Fig. 13a)[41]. High Wnt activity was mainly detected in TA cells. Mip-Seq analysis verified that in E16.5 incisor germs, most *Smoc2*+ cells are negative for *Axin2 or Lef1*, except in regions near the cervical loops (Supplementary Fig. 13b). These data indicate that *Smoc2* + MSCs normally reside in a low *Wnt* niche.

In contrast, increased *Axin2/Lef1* expression levels were observed in sequencing data of *Smoc1/2* DKO incisor mesenchyme (Fig. 6b, c). MIP-Seq further verified that the expression of *Axin2* and *Lef1* in the E16.5 mutant incisor was extended into the apical mesenchyme, where MSCs reside (Fig. 6d).

To analyze the functional significance of the canonical Wnt pathway, we generated *Smoc2-Cre^{ERT2}; Ctnnb1$^{flox/flox}$; Ai14* (Wnt inducible knockout/*Wnt* ICKO) and *Smoc2-Cre^{ERT2}; Ctnnb1-exon3$^{flox/+}$; Ai14* (Wnt inducible overexpression/*Wnt* IOE) mice and induced them with tamoxifen at E16. None of these mutants survived for very long, possibly due to systemic defects in other organs. *Wnt* ICKO pups died at P3.5, and significantly fewer tdTomato+ cells and a shorter migration distance were observed in the incisor mesenchyme compared to control littermate samples (Supplementary Fig. 13c). Ki67 staining showed that significantly less *Smoc2*+ cells were undergoing proliferation (Supplementary Fig. 13d, e). *Wnt* IOE pups died at birth, and significantly more tdTomato+ cells and a much longer migration pathway were observed in the apical incisor mesenchyme compared to control samples (Supplementary Fig. 13f). Strong ectopic Ki67 and Sp7 expression was detected in the apical mesenchyme of *Wnt* IOE incisors (Supplementary Fig. 13g, h).

These data indicate that the canonical Wnt pathway plays a critical role in regulating *Smoc2* + MSCs quiescence. *Smoc1/2* strongly inhibit Wnt activity and keep stem cells in a low Wnt *niche*.

SMOC1/2 are critical for WNT ligand trafficking

Next, we explore how *Smoc1/2* regulates canonical Wnt activity. WNT10a and WNT6 are the two most enriched canonical WNT ligands during incisor embryonic development[41,42]. ScRNA-seq data indicated that the RNA expression levels and ranges of these ligands showed no significant difference in DKO and wild-type control incisors at E16.5 (Fig. 6e). Mip-Seq data also showed that the RNA expression of Wnt6 and Wnt10a was detected in the distal pulp, odontoblasts, and dental epithelium of *Smoc1/2* DKO incisor germs with no detectable difference with the control incisors. No RNA expression of *Wnt10a* or *Wnt6* was detected in the apical pulp region (Fig. 6f, h, i). This indicates that the knockout of *Smoc1/2* had no effect to the RNA expression of *Wnt10a* and *Wnt6*.

Next, we performed immunofluorescent staining using antibodies against WNT10a and WNT6. In the control incisors, both WNT10a and

https://doi.org/10.1038/s41467-025-65705-z

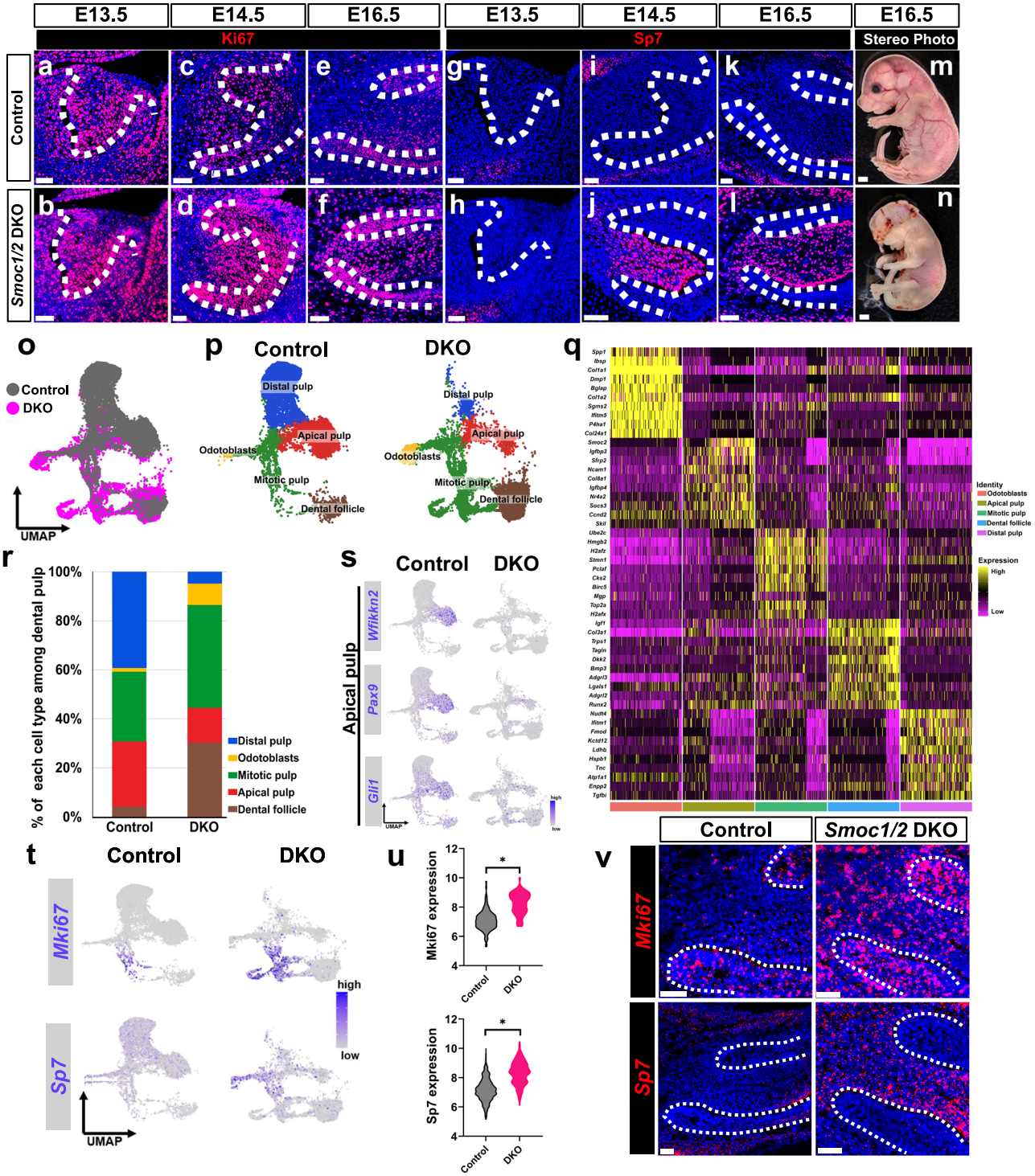

Fig. 5 | Loss of *Smoc1/2* leads to quiescence loss and mesenchymal hierarchy disruption. a–**l** Immunostaining of Ki67 and Sp7 in incisors of *Smoc2+/-* littermate control (control) and *Smoc1/2* DKO mice at E13.5, E14.5 and E16.5. **m**, **n** Images of control and *Smoc1/2* DKO embryos at E16.5. Scale bars: 50 μm in (**a**–**l**) and 1 cm in **m**, **n**. Representative images from three independent experiments with similar results. **o**–**s** Comparison of incisor mesenchymal populations in wild type control (control) and *Smoc1/2* DKO mice. **o**, **p** UMAP plot of the incisor mesenchyme of wild type and *Smoc1/2* DKO mice at E16.5. **q** Heatmap illustrating the top 10 differentially expressed genes between wild-type control and *Smoc1/2* DKO incisor mesenchymal clusters. **r** The percentage of mesenchymal cell types in control and *Smoc1/2* DKO mice. **s** UMAP feature plots in wild-type or *Smoc1/2* DKO mice embryo showed apical pulp signature genes expression nearly diminished in the mutant incisor. **t** Feature plots of *Mki67* and *Sp7* in control and *Smoc1/2* DKO incisor mesenchyme. **u** Quantitation of the expression level of *Mki67* and *Sp7* in individual cells within MSCs cluster of wild-type control and *Smoc1/2* DKO. Two-tailed Mann–Whitney U test; *Mki67*: control vs DKO, $p < 0.0001$; *Sp7*: control vs DKO, $p < 0.0001$. Source data are provided as a Source Data file. **v** Mip-seq showing the RNA probe signals of *Mki67* and *Sp7* in the incisor of control and *Smoc1/2* DKO mice. Scale bars: 50 μm. Representative images from three independent experiments with similar results.

https://doi.org/10.1038/s41467-025-65705-z

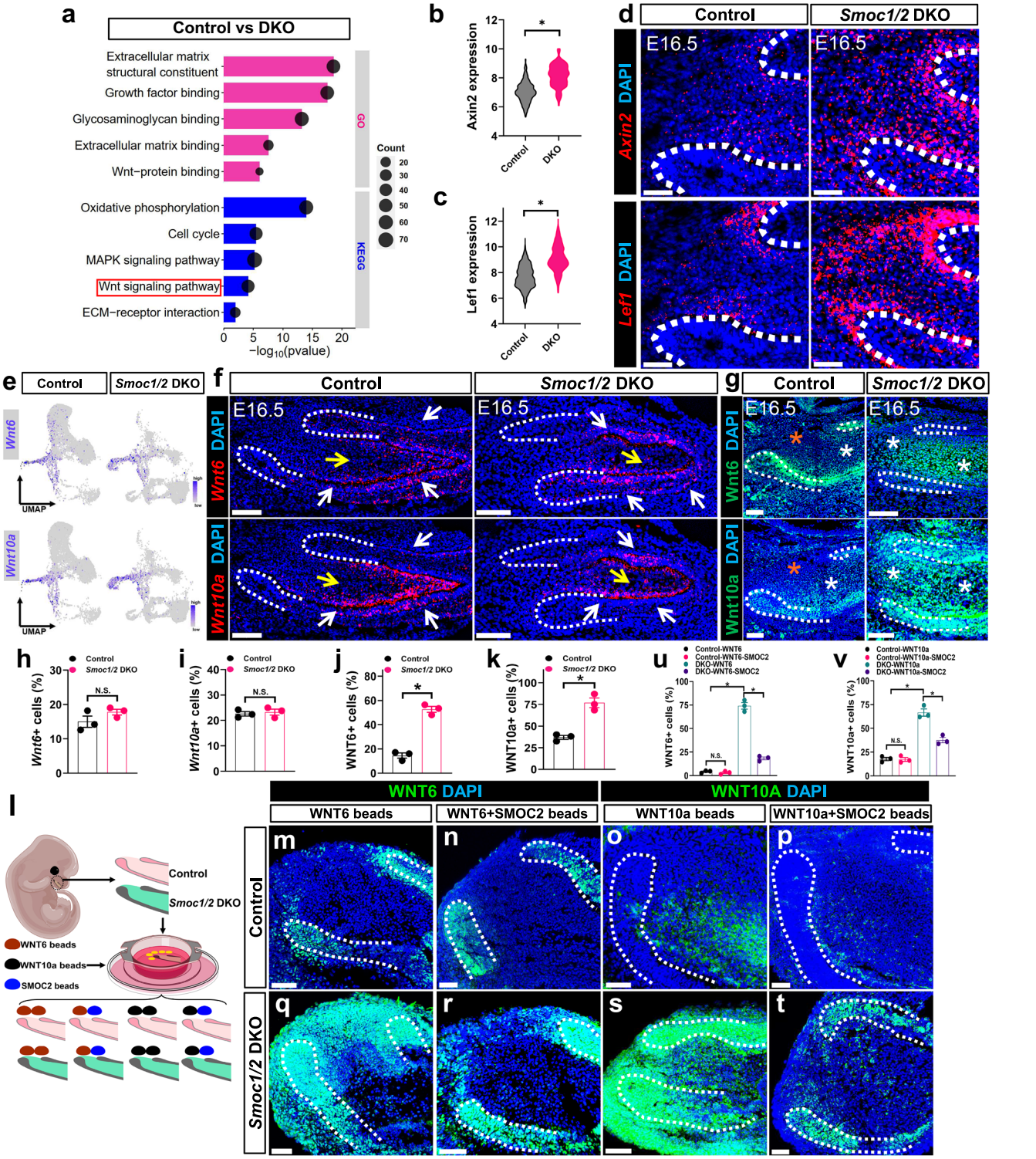

WNT6 proteins were detected in the distal pulp and odontoblast regions, while no signal was observed in the apical pulp region. In contrast, in the *Smoc1/2* DKO incisor germ, robust immunofluorescent signals for both WNT10a and WNT6 were detected in the apical region (Fig. 6g, j, k). This indicates that knockout of *Smoc1/2* leads to the redistribution of WNT10a and WNT6 proteins to the proximal region of the incisor pulp.

The difference between RNA expression and immunostaining patterns suggests that SMOC1 and SMOC2, two extracellular matrix (ECM) molecules, may affect the distribution of WNT ligands within the niche without altering their expression. To further verify this, we conducted bead explant assays on tooth germ organ cultures[25] (Fig. 6l). Incisor germs from E16.5 DKO or wild-type mouse embryos were co-cultured with beads coated with WNT ligands, with or without SMOC2-coated beads in the apical region. In wild-type samples, the addition of exogenous WNT10a or WNT6 beads, with or without SMOC2 beads, did not increase the WNT6/10a protein level in the apical pulp region (Fig. 6m-p). In contrast, in *Smoc1/2* DKO incisor explants, the addition of WNT10a or WNT6 beads significantly increased the protein levels of WNT6 or WNT10a in the apical region (Fig. 6q, s). The presence of SMOC2-coated beads significantly reduced the WNT protein levels in the apical pulp regions (Fig. 6r, t–v). Further,

Fig. 6 | SMOC1/2 are critical for WNT ligand trafficking and prevent canonical WNT ligands from accessing mesenchymal stem cells. a–**d** Knockout of *Smoc1/2* leads to elevated Wnt activity. **a** Gene Ontology and KEGG analyses of differentially expressed genes in the mesenchyme of control versus *Smoc1/2* DKO incisors at E16.5. **b**, **c** Quantitation of expression levels of *Axin2* and *Lef* within individual apical pulp cells of *Smoc2*+/- littermate control and *Smoc1/2* DKO. Two-tailed Mann−Whitney U test; *Axin2*: control vs DKO, $p < 0.0001$; *Lef1*: control vs DKO, $p < 0.0001$. **d** Mip-seq analysis showing RNA expression of *Axin2* and *Lef1* in the incisor of control and *Smoc1/2* DKO mice. Scale bars: 50 µm. Representative images from three independent experiments with similar results. **e**–**g** Knockout of *Smoc1/2* did not significantly affect *Wnt6* and *Wnt10a* RNA levels but changed their protein distribution. **e** UMAP feature plots showed comparable transcription levels of Wnt6 and Wnt10a in control versus *Smoc1/2* DKO incisors at E16.5. **f** MIP-seq data showed similar RNA expression levels and patterns of *Wnt6* and *Wnt10a* in incisors of *Smoc2* + /- littermate controls and *Smoc1/2* DKO mice embryos at E16.5. **g** Antibody staining of WNT6 and WNT10a in incisors of *Smoc2* + /- littermate control and *Smoc1/2* KO embryos at E16.5. Scale bars: 100 µm. White arrows indicate RNA probe signals in incisor epithelium, while yellow arrows show RNA probe signals in incisors mesenchyme. White asterisks indicate positive immunostaining signals, while yellow asterisks show low signals in the apical pulp regions of incisors. Representative images from three independent experiments with similar results. **h**, **i** Quantitation of panels (**f**) revealed no significant difference in the percentage of cells expressing *Wnt6* or *Wnt10a* RNA between control and *Smoc1/2* DKO mice incisors. **j**, **k** Quantitation of **g** showed significantly more pulp cells positive for WNT6+ and WNT10a+ immunostaining in *Smoc1/2* DKO mice incisors compared to controls. Data are presented as mean ± SEM. $n = 3$ biological replicates; unpaired two-tailed Student's t-test. *Wnt6*+ cell: control vs DKO, $p = 0.2071$; *Wn10a*+ cell: control vs DKO, $p = 0.6739$, WNT6+ cell: control vs DKO, $p = 0.0003$; WNT10a+ cell: control vs DKO, $p = 0.0026$; N.S.: not significant. **l**–**v** Organ culture of incisor tooth germs at E16.5. **l** The schematic drawing illustrates the experimental scheme for the explant culture. Created with MedPeer (medpeer.cn). Organ culture experiments were conducted using wild-type control incisor explants incubated with WNT6 beads (**m**), WNT6 + SMOC2 beads (**n**), WNT10a beads (**o**), or WNT10a + SMOC2 beads (**p**). The samples were subsequently stained with WNT6 or WNT10a antibodies, respectively, and the staining results were quantified in (**u**). **q**–**t** Similar beads explant experiments were performed using *Smoc1/2* DKO incisor embryos at E16.5, and the results were quantified in (**v**). Data are presented as mean ± SEM. $n = 3$ biological replicates; unpaired two-tailed Student's *t*-test. WNT6+ cell: control-WNT6 vs control-WNT6-SMOC2, $p = 0.4189$, control-WNT6 vs DKO-WNT6, $p < 0.0001$, DKO-WNT6 vs DKO-WNT6-SMOC2, $p = 0.0001$; WNT10a+ cell: control-WNT10a vs control-WNT10a-SMOC2, $p = 0.8690$, control-WNT10a vs DKO-WNT10a, $p = 0.0003$, DKO-WNT10a vs DKO-WNT10a-SMOC2, $p = 0.00$; N.S.: not significant. Source data are provided as a Source Data file.

immunostaining for Lef1 and Ki67 revealed that DKO explants exposed to Wnt ligands exhibited significant increases in both Lef1+ and Ki67+ cells in the apical pulp compared to controls, confirming hyperactive Wnt signaling (Supplementary Fig. 14). Notably, supplementation with SMOC2-coated beads partially reduced Lef1 and Ki67 levels in *Smoc1/2* DKO explants.

These data directly demonstrate that *Smoc1/2* deficiency enhances incisor pulp sensitivity to Wnt ligands, indicating that SMOC1/2 ECM proteins inhibit the trafficking of canonical WNT ligands within dental mesenchyme.

SMOC1/2 disrupt the binding between WNT ligands and glypican

Next, we sought to explore how SMOC1/2 inhibit canonical WNT ligand trafficking using in vitro approaches. To verify the role of SMOC1/2 in regulating the Wnt signaling pathway, we overexpressed *Smoc1* or *Smoc2* in dental pulp cells (DPCs), isolated from E16.5 mouse tooth germs. Overexpression of either *Smoc1* or *Smoc2* suppressed the expression of active β-catenin and its downstream targets, including c-Myc, Cyclin D1, and LEF1, indicating inhibition of the canonical Wnt/β-catenin pathway (Fig. 7a). Notably, combined overexpression of *Smoc1* and *Smoc2* resulted in a stronger inhibitory effect on β-catenin signaling, suggesting an additive effect when both SMOC1 and SMOC2 are present (Fig. 7b). Furthermore, the nuclear translocation of β-Catenin induced by the Wnt agonist WAY, a hallmark for Wnt/β-catenin signaling activation, was blocked by *Smoc1* or *Smoc2* overexpression (Fig. 7c).

We designed an in vitro assay to examine whether SMOC affects the WNT ligand trafficking process (Fig. 7d). Control DPCs were co-cultured with WNT10a beads and BSA beads. WNT10a protein released from the beads was able to diffuse and bind to surrounding cells, as visualized by WNT10a immunostaining. This demonstrates the normal spread of WNT10a from a localized source. In contrast, when DPCs were co-cultured with WNT10a beads alongside SMOC1 or SMOC2 beads, a striking difference was observed. The cells in the vicinity of the SMOC1 or SMOC2 beads showed a significant reduction or complete absence of WNT10a immunostaining (Fig. 7e). Importantly, the WNT10a beads themselves remained positive for WNT10a immunostaining, indicating that the ligand was still present and being released, but its spread to neighboring cells was impeded by the localized presence of SMOC1 or SMOC2. This assay demonstrated that SMOC1 and SMOC2 can interfere with Wnt10a transportation.

WNT ligands are highly hydrophobic and rely on carrier proteins to spread in the aqueous extracellular space[43,44]. In Drosophila, Glypican (GPC) plays critical roles in the transportation of WNT ligands, which bind to WNT and provide a hydrophobic space to facilitate their trafficking[45]. To investigate the correlation between *Gpc6* expression and *Smoc1/2*, *Wnt10a*, and *Wnt6*, we performed Mip-seq RNA imaging and immunofluorescence analysis (Supplementary Fig. 15). These experiments revealed that *Gpc6* is widely expressed in incisor epithelium and mesenchyme. To determine if GPC also modulates WNT ligand trafficking in mammals, we silenced *Gpc6* using siRNA. As a result, the expression of active β-catenin and its downstream targets c-Myc, Cyclin D1, and LEF1 was significantly suppressed after *Gpc6* knockdown (Fig. 7f). Additionally, the nuclear translocation of β-catenin induced by WAY treatment was also blocked following *Gpc6* silencing (Fig. 7g).

Next, we examined whether SMOC1/2 regulated the expression of GPC6. Our findings revealed that the overexpression of *Smoc1*, but not *Smoc2*, slightly downregulated the expression of GPC6 (Supplementary Fig. 16a). Both SMOC1 and SMOC2 bind to GPC6 in DPCs, as assessed by Co-immunoprecipitation (Co-IP) assay (Fig. 7h). This interaction was further validated by immunofluorescence staining, which showed the colocalization of SMOC1/2 and GPC6 in DPCs (Fig. 7i).

Next, we evaluated interactions among SMOC1/2, WNT10a, and GPC6. Co-IP experiment showed binding between GPC6 with WNT10a was disrupted by the presence of either SMOC1 or SMOC2 (Fig. 7j). Quantitative Fluorescence Resonance Energy Transfer (FRET) analysis further verified that the binding affinity between WNT10a and GPC6 was reduced by more than fivefold in the presence of SMOC2 (Supplementary Fig. 16b, c).

These findings indicate that SMOC1/2 inhibit WNT trafficking by competitively binding to GPC6, thereby disrupting WNT ligand distribution within the niche (Fig. 7k).

Discussion

Using mouse incisor as a model, our study provided answers to several questions for the developmental biology of stem cells. We found that MSCs in mouse incisors establish their identity between E14.5 and E16.5 and persist into adulthood. Rather than simply maintaining an embryonic state, they arise through an inductive process that acquires quiescence via an autocrine *Wnt* inhibition mechanism. Furthermore, a

https://doi.org/10.1038/s41467-025-65705-z

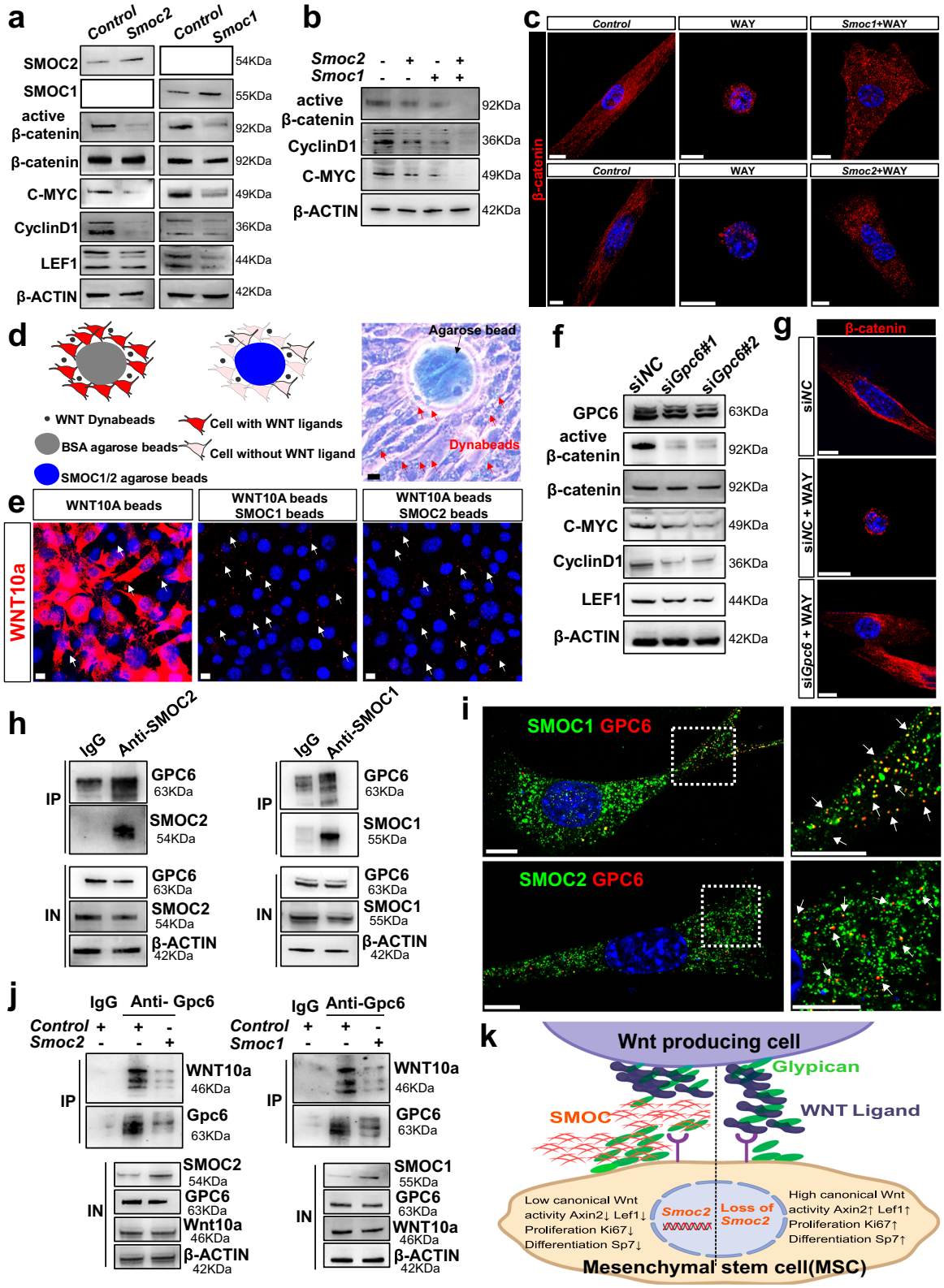

common stem cell population supports both developmental and adult incisor formation.

Dental mesenchyme develops from cranial neural crest cells, which are known to be a group of multipotent cells migrating out of the neural tube[46]. Cranial neural crest cells eventually give rise to diversified tissue types, including craniofacial bones, teeth, fat, ganglion neurons, glia cells, and melanocytes[47]. Due to their multi-differentiation capability, cranial neural crest cells have also been referred to as neural crest stem cells[47]. An obvious challenge is to distinguish embryonic progenitors from adult stem cells[8]. Alternatively, when can we consider stem cells as stem cells during development? The core features of adult stem cells include self-maintenance, multi/mono lineage contribution capability, and quiescence. Although actively cycling stem cells have been identified in some organs, like the intestine and skin, quiescence is still a fundamental characteristic for defining stem cells[48–50]. Quiescent stem cells

Fig. 7 | SMOC1/2 inhibit canonical *Wnt* activity by competitive binding to trafficking protein *Gpc6*. **a** Expression of active β-Catenin and its downstream targets c-Myc, Cyclin D1, and LEF1 in DPCs after *Smoc1* or *Smoc2* overexpression, as assessed by western blot. **b** Expression level of active β-Catenin and its downstream targets c-Myc, and Cyclin D1 in DPCs after *Smoc1/2* overexpression alone or simultaneously. **c** Immunostaining of β-Catenin in control, Wnt agonist WAY and WAY with *Smoc1/2* treated groups. Scale bars: 10 μm. Representative images from three independent experiments with similar results. SMOC1/2 interfere with Wnt10a transportation. **d** The schematic drawing illustrates the experimental scheme of DPCs supplied with beads. Created with MedPeer (medpeer.cn). **e** Immunostaining of Wnt10a in cultured DPCs supplied with beads. White arrows indicate WNT Dynabeads. Scale bars: 10 μm. Representative images from three independent experiments with similar results. **f** Expression of active β-Catenin and its downstream targets c-Myc, Cyclin D1, and LEF1 in DPCs after *Gpc6* silencing, as assessed by western blot. **g** Immunostaining of β-Catenin in siRNA negative control (si*NC*), WAY with si*NC* and WAY with si*Gpc6* treated groups. Scale bars: 10 μm. Representative images from three independent experiments with similar results. **h** Co-IP of GPC6 with SMOC1 or SMOC2 in DPCs. **i** Co-localization analysis of SMOC1/2 with GPC6, as assessed by immunostaining. White arrows indicate co-localization signals. Scale bars: 10 μm. Representative images from three independent experiments with similar results. **j** Co-IP of GPC6 with WNT10a in DPCs in *control*, *Smoc2* or *Smoc1* overexpression groups. Source data are provided as a Source Data file. **k** Mechanism diagram. SMOC1/2 inhibit WNT trafficking by competitively binding to GPC6, thereby disrupting WNT ligand distribution within the niche. Created with MedPeer (medpeer.cn).

remain out of the cell cycle but retain the proliferation capacity[51]. By maintaining quiescence, stem cells can retain their life-long tissue homeostasis and regenerative capacity. Loss of quiescence severely disrupts tissue homeostasis and stem cell maintenance[38,52,53]. In contrast, progenitor cells in embryonic tissue undergo active cell divisions[8]. As shown in our study, at E13.5, nearly all mesenchymal cells are undergoing proliferation. This is also commonly observed in embryonic progenitors of many other tissue types[3,54,55]. Therefore, the establishment of quiescence, but not multipotential capability, is the key feature to distinguish stem cells from embryonic progenitors.

Completion of the lineage hierarchy is another criterion to justify the establishment of stem cells during development. Adult organs and tissues are composed of cells at various differentiation stages. Despite constant turnover, the hierarchical architecture remains constant throughout the lifetime, as seen in the intestine, blood, and skin, among others[56]. The pulp mesenchyme of adult mouse incisors is composed of five compartments, including mesenchymal stem cells (apical pulp), transit-amplifying (TA) cells (mitotic pulp), distal pulp, and differentiated odontoblasts[24,57]. In molar development, the dental mesenchyme segregates from a homogeneous population at E13.5 into two components at E14.5 and then into four components at E16.5[34]. Our study shows that a similar segregation process occurs in the incisor mesenchyme between E14.5 and E16.5. The five-compartment hierarchy, along with the quiescence and quantity of stem cells, is maintained into adulthood throughout the lifetime. While the emergence of *Smoc2* expression within this timeframe is relevant, it is not a determining factor for defining the stem cell population. Our conclusion that stem cell identity is established during this developmental window remains valid based on our sequential sequencing analysis, independent of *Smoc2* as a marker. Therefore, we define E16.5 as the time point when MSCs establish their identity. MSCs continue to evolve after birth. *Smoc2*+ cells at E16.5 contribute significantly to periodontal tissue, whereas adult *Smoc2*+ cells make only a minor contribution, suggesting that multipotency is further restricted during postnatal development.

A technical challenge in studying the stem cells development is to identify a stem cell marker in embryonic stages. Since its identification in the mouse incisor, *Gli1* has become the most widely used marker for MSCs across various organs and tissues[58–61]. *Gli1* is broadly expressed throughout the entire embryonic craniofacial mesenchyme, which limits its utility in studying MSC development[23]. Importantly, *Gli1*+ MSCs comprise a heterogeneous population, including dormant MSCs, primed MSCs and glial cells within neurovascular bundles. We hypothesize that *Gli1*+/*Smoc2*+ cells represent the dormant MSC subset. The *Gli1*+;*Smoc2*- population likely contains primed stem cells capable of rapid differentiation and provides an immediate supply to support mesenchymal turnover. The neurovascular-associated *Gli1*+ glial cells may directly contribute to central pulp labeling[62]. The significantly slower contribution rate of *Smoc2*+ cells is consistent with their quiescent state, while their dominant long-term contribution (>80%) underscores their functional importance. Identification of *Smoc2*+ quiescent subpopulation as the major contributing subset demonstrates functional heterogeneity within a stem cell pool and provides a foundation for dissecting transitions between quiescent, primed, and potentially other states within the *Gli1*+MSC compartment. Further experiments are needed to investigate the stem cells heterogeneity.

Smoc1/2 are ECM glycoproteins belonging to the SPARC/osteonectin family. They have been shown to regulate osteogenic differentiation downstream of the BMP/*Runx2* signaling pathway[40]. While some studies have suggested their association with congenital human diseases and cancer progression, the functions of *Smoc1/2* remain largely unexplored[63–65]. Our study reveals the function of these proteins as potent Wnt inhibitors.

In *Smoc1/2* KO mutant tooth germs, although the RNA expression pattern and level of WNT ligands remain unchanged, immunostaining showed that WNT proteins dramatically extended their distribution range, indicating disrupted trafficking. In incisor mesenchyme, *Wnt6* and *Wnt10a*, the two major canonical WNT ligands, are mainly secreted by odontoblast, distal pulp, and dental epithelium, which are at a distance from the stem cells at the apical region. WNT ligands are hydrophobic proteins that are insoluble in aqueous solutions[43]. Various mechanisms have been proposed to explain how hydrophobic Wnt proteins propagate across the extracellular space to access target cells[66,67]. In Drosophila, glypicans (GPCs) are critical for the extracellular distribution of Wingless (Wnt). Glypicans such as Dally and Dally-like protein (Dlp) bind to Wnt ligands and contribute to their spread by shielding the lipid moiety, allowing signaling to occur efficiently[45]. Our study shows that in mice, GPC6 interacts with SMOC1/2 in a competitive manner, inhibiting GPC6 from binding to WNT10a. This interaction plays a key role in regulating the trafficking of the Wnt ligand. Pentagone (Pent), the homolog of SMOC2 in Drosophila, was known to interact with the glypican Dally and Dlp to control Decapentaplegic (Dpp) distribution[68,69]. Our study showed that SMOC1/2 can also bind to GPC6 directly to inhibit WNT ligand trafficking. Interestingly, while Drosophila Dlp and Dally have similar structures, only Dlp exhibits lipid-binding activity[45]. Whether other GPC family members participate in Wnt ligand trafficking needs further study.

The reciprocal interactions between epithelial and mesenchymal tissues are critical for tooth development, with epithelial WNT signaling dynamics heavily influenced by mesenchymal cues. The epithelial abnormalities in *Smoc1/2* DKO mice are likely a secondary defect due to disrupted mesenchymal-to-epithelial signaling, which was known to be critical for tooth development[70]. In addition, most ECM proteins typically exhibit longer half-lives than intracellular proteins, enabling them to maintain tissue structural integrity over broader areas[71]. Consequently, the regulatory effects of mesenchymal SMOC1/2 ECM proteins might extend beyond incisor mesenchyme into the epithelium.

Our findings provide a new perspective on understanding how ECM proteins inhibit Wnt activities within the stem cell niche[72]. Notably, this mechanism may also apply to other signaling pathways, as

both SMOCs and GPCs are known to regulate other ligand trafficking processes, including BMPs, FGFs, and Hedgehog ligands[69,73,74].

Knockout of *Smoc1/2* resulted in not only tooth phenotypes but also severe craniofacial bone loss, long bone defects as well as defects in vasculature and hair follicles, suggesting their critical roles in other organs[40]. In fact, *Smoc2* has also been shown to be markers for intestinal stem cells and gastric cancer stem cells[1,75]. Although we propose *Smoc1/2* play complementary roles during prenatal MSC development, based on their largely overlapping expression in embryonic mesenchyme, their diverging expression patterns after birth and the distinct phenotypes observed in *Smoc1 KO* and *Smoc2 KO* mutant mice indicate divergent functions in postnatal development.

Methods

Animals

All animal care and experimental procedures were conducted with the approval of the Animal Care and Use Committee of the Chinese Institute for Brain Research, Beijing (CIBR), in accordance with the governmental regulations of China. All mouse strains were maintained on a predominantly C57BL/6 background. Sex was not considered as a biological variable in this study. Animals were housed in 12-hour light/dark cycles at 23 ± 1 °C and humidity 60 ± 5%. Food and water were provided ad libitum. Mice at postnatal day 56 or at least 6-8 weeks old were used for experiments. *Gli1-CreERT2* (JAX#007913), *Ai14* tdTomato reporter (JAX#007908) and *β-Catenin* $^{flox/flox}$ (JAX#004152) mice were purchased from the Jackson Laboratory. *Smoc1*-KO (#T037738), *Smoc1*^{flox} (#T037703) and *Smoc2*^{flox} (#T020166) mice were purchased from GemPharmatech. *Ctnnb1*$^{flox(ex3)}$ was kindly provided by Dr. Woo-Ping Ge at CIBR.*Gli1-GFP* mice were generously shared by Dr. Bo Shen, National Institute of Biological Science. *Smoc2-CreERT2*, *Smoc2*-KO and *Smoc2-mScarlet* mouse line were generated at the CIBR Genetic Manipulation Core (described in 'Generation of *Smoc2-CreERT2*, *Smoc2*-KO and *Smoc2-mScarlet* mice' below). *Gli1-CreERT2*, *Smoc2-CreERT2* and *Smoc2-mScarlet* mice used for both breeding and experiments were heterozygous, and all *Smoc1*-KO and *Smoc2*-KO used for breeding were heterozygous. Timed embryos were obtained by heterozygous matings counting the vaginal plug as E0.5 and using morphological criteria for precise staging. The *Smoc1*/2-DKO homozygous mutant embryos can easily be identified from E16.5 because of the severe dysplasia phenotype. Only wild-type and *Smoc1*/2-DKO homozygous littermates were used as donors for experiment.

Generation of *Smoc2-CreERT2* mice

Smoc2-CreERT2 mice were generated by homologous recombination at the endogenous *Smoc2* locus with the help of the CRISPR/Cas9 system. Briefly, we inserted *P2A-CreERT2* before the stop codon TGA of the *Smoc2* gene. The sgRNA was designed near the stop codon. The sgRNA synthesis template was obtained by PCR and purified using the Qiagen MinElute kit with the T7 promoter. The sgRNA sequences were 5′-AAGACAGTTCCTAGACATGT-3′ and 5′-CAAGACAGTTCCTAGACATG-3′., and *CreERT2* was amplified from addgene13777 by PCR. P2A was added upstream of *CreERT2* through primers, and these fragments were cloned into the pCE-Zero vector in the order of 5′ homology arm-P2A-*CreERT2*-3′ homology arm. A mixture of donor DNA plasmid, sgRNA and Cas9 mRNA was microinjected into fertilized zygotes from C57BL/6 J females. Injected zygotes were implanted into oviducts of pseudopregnant ICR female mice. The genotyping primers were 5′-GCCGAGCTCTCTATGACTCT −3′and 5′- CTTGCGAACCTCATCACTCG −3′. Any potential off-target effects were bred out by backcrossing to C57BL/6 mice for at least five generations before the mice were used for experiments.

Generation of *Smoc2-mScarlet* mice

Smoc2-mScarlet mice were generated by replacing approximately 3.3 kb of the gene starting from the ATG initiation codon with *mScarlet-P2A-mScarlet-T2A-mScarlet-WPRE-pA* using the CRISPR/Cas9 system. The sgRNA was designed in the start codon and the first intron. The sgRNA sequences were 5′-GGCAGCCAGCACAGCTGTGG-3′ and 5′-GCCAGGATGATAGGATGTGG-3′. PCR was used to amplify the 5′ and 3′ homology arms from wild-type mouse gDNA, and *mScarletX3-WPRE-pA* was obtained by restriction enzyme digestion from a template plasmid. These fragments were then cloned into the pSK vector. A mixture of vector, sgRNA, and Cas9 mRNA was microinjected into fertilized zygotes from C57BL/6 J females. F0 and F1 mice were genotyped through PCR to ensure the presence of recombination. The genotyping primers were 5′-TAGTTGCCAGCCATCTGTTG-3′ and 5′-CTCCCCACACAGAGGATGTT-3′. Any potential off-target effects were bred out by backcrossing to C57BL/6 mice for at least five generations before the mice were used for experiments.

Generation of *Smoc2*-KO mice

Smoc2 knock-out mice were constructed with CRISPR-Cas9 gene targeting technology. To delete the entire coding region of *Smoc2*, one sgRNA was designed near the start codon and another after the stop codon. The sgRNA sequences were 5′-GGCAGCCAGCACAGCTGTGG-3′ and 5′-ACTTCCTCGTCCCTCTGTGG-3′. A mixture of Cas9 mRNA and sgRNAs was injected into fertilized eggs through electroporation, and the eggs were then transplanted into the womb of foster mothers. F0 and F1 mice were genotyped through PCR to ensure the presence of recombination. The genotyping primers were 5′- GGGAAAC-TAGGGCTGTTTGA −3′ and 5′ - ATGCCTGAGCTAGTGCCTGT −3′. Any potential off-target effects were bred out by backcrossing to C57BL/6 mice for at least five generations before the mice were used for experiments.

Tamoxifen administration

Tamoxifen was dissolved in corn oil at 20 mg/ml as a working solution. Mice were injected intraperitoneally at a dosage of 1.5 mg/10 g body weight. For embryonic induction, the timed pregnancy was determined by identifying a vaginal plug (E0.5), and then tamoxifen was administered intraperitoneally to the pregnant females at the target embryonic day. For in vivo colony tracing assay, mice were injected with tamoxifen intraperitoneally at a dosage of 1 μg/g body weight once[61]. For postnatal studies of embryonically induced mice, live embryos were recovered by cesarean section at E19.5 in case the pregnant mice did not give birth naturally, and then fostered and raised by a non-biological mother.

EdU and BrdU administration

The protocol for labeling EdU-labeled LRCs and BrdU-labeled fast-cycling cells was adapted from previous[31,32]. Briefly, mice were given an intraperitoneal injection of 2 mg/10 g body weight of EdU (ST067, Beyotime) or BrdU (ST1056, Beyotime) and then harvested at various timepoints after administration (label timepoints are provided in the main text). EdU detection kit (C0071L, Beyotime) was used to detect EdU following the manufacturer's protocol.

Incisor injury

The incisor injury protocol was adapted from a previous study[23]. Briefly, separate the masseter muscle on one side of the mouse to expose the apical bone surface of the mandibular incisor, puncture the apical region of the incisor pulp with a 23G needle to create an injury, while the contralateral mandibular incisor serves as a control. After injury, mice were housed individually and provided with soft food for 3 days.

Cell culture and differentiation

Incisor pulp was obtained from E16.5 *Smoc2-CreERT2; Ai14* and *Smoc2-mScarlet* mouse embryos. The pulp tissue was minced into pieces and digested with type I collagenase (3 mg/ml), Dispase (4 mg/ml), and

DNase I (1 U/ml) at 37 °C for 30 min, followed by collagenase inactivation with 2% FBS. The digested tissue was disrupted using a 1 pipette tip and then centrifuged at 400 × g for 5 min. Cells were resuspended in HBSS (pH 8.0) containing 2% FBS. Then, cell suspensions were filtered through a 40 μm mesh (BD Falcon). Isolated cells were cultured in DMEM low glucose supplemented with 20% FBS 2 mM glutamate, and 1% penicillin/streptomycin (Invitrogen) at 37 °C in regular atmospheric conditions. For clonal culture, cells were seeded at 5×10^4/well in a 6-well plate for 21 days. Colonies consisting of more than 50 cells were counted as a colony cluster. For the differentiation assays, cells were seeded at 1×10^5/well in a 12-well plate and cultured until confluent and then induced in osteogenic, adipogenic or chondrogenic differentiation medium (StemPro Differentiation kits, Gibco) according to the manufacturer's protocols for 14 days.

Sample preparation for sectioning

Samples for paraffin sectioning were fixed in 4% PFA and decalcified with 10% EDTA as needed. Then, samples were dehydrated with serial ethanol solutions (50%, 70%, 80%, 90% and 100%) at room temperature, followed by xylene. After being embedded in paraffin wax, sections were cut to 5 mm on a microtome (Leica). Cryosectioning samples were fixed and decalcified in the same way as samples prepared for paraffin sectioning. 30% sucrose was used for the dehydration of the samples. Then, samples were embedded in OCT compound (Tissue-Tek) and cut to 10–12 mm on a cryostat (Leica).

Histological analysis

Hematoxylin and Eosin staining were performed using the standard protocol. Paraffin sections prepared as described above were used for histological analysis. Images were acquired using an epifluorescence microscope (Olympus VS120) with a 20× objective lens.

Immunostaining

Cryosections and paraffin sections prepared as described above were used for immunofluorescence assays. Briefly, sections were dried for 2 hours at 60 °C. Then, paraffin sections were deparaffinized and rehydrated before antigen retrieval (H-3300, Vector). Samples were then washed three times with PBST (0.1% Tween20 in 1xPBS) followed by 1 hour blocking at room temperature (FP1020, PerkinElmer). For cells, the pre-fixed cells in 4% PFA were permeabilized in 0.05% TritonX-100 (BioRuler, 9002-93-1) for 10 min at room temperature, and then blocked at room temperature for 1 hour. Then, cells or sections were incubated with primary antibodies diluted in the blocking buffer overnight at 4 °C. After washing with PBS, samples were incubated with secondary antibodies diluted in the blocking buffer at room temperature for 2 hours. DAPI (Sigma, D9542) was used for nuclear staining. Olympus VS120, Leica SP8 confocal microscope, and Zeiss LSM 880 confocal microscope were used to acquire images. The following is a list of the primary antibodies that were used: Ki67 (Abcam, ab15580; 1:200), Sp7 (Abcam, ab209484; 1:200), Col1 (Abcam, ab21286; 1:500), αSMA (Abcam, ab5694 1:100), β3-tubulin (Abcam, ab78078, 1:1,000), BrdU (Invitrogen, B35128, 1:100), Lef1 (HUABIO, HA500273, 1:100), Gpc6 (OriGene, TA351222S, 1:100), Wnt6 (ProteinTech, 24201-1-AP; 1:100), Wnt10a (Abcam, ab106522; 1:100), β-catenin (Cell Signaling Technology, 8480; 1:100), Smoc1 (Santa Cruz Biotechnology, sc-390448; 1:50) and Smoc2 (Santa Cruz Biotechnology, sc376104; 1:50). Secondary antibodies were Invitrogen Alexa Fluor 488/568/647 used at 1:500 dilution.

RNAscope imaging

Cryosections were used for RNAscope. Briefly, samples were fixed in 4% PFA in DEPC-treated PBS at 4 °C for 8 hours and decalcified with 10% DEPC-treated EDTA as needed. DEPC-treated 30% sucrose was used for dehydration of the samples. Then samples were embedded in OCT compound and cut into 8–10 mm sections. The signal of *Smoc1* and *Smoc2* mRNA was detected using RNAscope multiplex fluorescent v2 assay (323100, Advanced Cell Diagnostics) according to the manufacturer's protocol. RNAscope probes used in this study included: *Smoc1* (571511-C2, Advanced Cell Diagnostics), *Smoc2* (318541-C3, Advanced Cell Diagnostics).

Mip-seq method for detecting multiple mRNAs on one cryosection

Detection of multiple mRNA in one cryosection was performed via Mip-seq[37]. Briefly, cryosections were sealed within Secure-Seal hybridization chambers (621201, Grace Bio-Labs) to perform the following reactions. Samples were rinsed twice with DEPC-treated PBS. After dehydration and denaturation of samples with methanol, the hybridization buffer containing specific targeting probes was added to the chambers for incubation at 37 °C overnight. Then samples were washed three times with PBST, followed by ligation of targeting probes in the ligation mix at 25 °C for 3 hours. Next, samples were washed three times with PBST and subjected to rolling circle amplification by Phi29 DNA polymerase at 30 °C overnight. Subsequently, the probes with different fluorophores (Alexa 488, Cy3, Cy5, and Cy7) in hybridization buffer were applied to the samples. Next, samples were dehydrated with an ethanol series and mounted with mounting medium. The samples were then thrice washed using a 10% formamide in 2X SSC solution, followed by DAPI staining. Imaging was conducted on a Leica THUNDER Imaging Systems, 20× (NA = 0.80). After each imaging round, signals were eradicated with a stripping buffer (60% formamide in 2X SSC) twice for 10 minutes at room temperature. This was followed by the addition of the subsequent rounds of probes to conduct multiple rounds of hybridization and imaging. The probes used in this study included: *Aldh1a2, Dpep1, Epha3, Bmp3, Ntn1, Smoc1, Smoc2, Pax9, Wfikkn2, Nell1, Mki67, Cdk1, Plk1, Bub1, Fgf3, Dspp, Alpl, Sp7, Col1a1, Dmp1, Fmod, Dll1, Tgfb3, Stc2, Gpc5, Gpc6, Runx2, Axin2, Lef1, Wnt4, Wnt5a, Wnt5b, Wnt6, Wnt9a, Wnt10a* and *Wnt11*.

Single-cell RNA barcoding and sequencing

Single-cell transcriptomes were obtained from the digestion of the incisor pulp at different stages (E13.5, E14.5, E15.5, E16.5, E18.5, and P56). In brief, the isolated incisor pulp or germ with dental epithelium and surrounding dental follicle were placed in 4 mg/ml Dispase and 3 mg/ml Collagenase I on a thermomixer at 37 °C for 15 to 30 min depending on the stage of the sample, to release cells from the tissue. All our samples had more than 85% viable cells. For E13.5, E14.5, E15.5, E16.5, E18.5, and P56 wild-type mice incisors, libraries were prepared using SeekOne Digital Droplet Single-Cell 3′ library preparation kit (SeekGene). For *Smoc1/2* DKO and wild-type control incisors, libraries were prepared using Single Cell 3′ Library Kit v2 (PN-120236/37/62, 10X Genomics). The numbers of actually sequenced cells were 16101 cells for E13.5, 23469 cells for E14.5, 17053 cells for E15.5, 15828 cells for E16.5, 13806 cells for E18.5, 24704 cells for P56, 30292 cells for E16.5 *Smoc1/2* DKO, and 26017 cells for wild-type control incisor. Quality control, mapping, and count table assembly of the library were performed using the CellRanger pipeline.

ScRNA-seq data clean-up and normalization

Raw read counts from the cells at each stage were analyzed using the Seurat 4.0 R package. Low gene expression cells were filtered out following standard Seurat object generation. Cells with fewer than 200 genes and mitochondrial gene percentages >50 were removed. Sctransform was applied for normalization and cell cycle regression.

Analysis of scRNA-seq data

Identifying variable genes and dimensionality reduction. RunPCA and RunUMAP were performed for dimensionality reduction and visualization of the clustering.

Subcluster analysis. Subcluster analysis was performed to investigate the heterogeneity within the dental mesenchymal populations. A combination of marker genes identified from published literature was used for identifying the dental mesenchymal cell populations in the mouse incisor[24].

Integrative analysis of different samples. Seurat 4 was used to combine the single-cell data of different samples and perform integration analysis. The PrepSCTIntegration function was performed before identifying anchors with the function FindIntegrationAnchors. Seurat objects were then returned by passing these anchors to the Integrate Data function. RunPCA and RunUMAP visualization were used for downstream analysis and visualization.

Monocle trajectory analysis. Monocle3 was applied to generate the pseudotime trajectory across the dental mesenchymal cells. The cells were input to Monocle3 to infer cluster and lineage relationships within a given cell type. UMAP embeddings and cell subclusters generated from Seurat were converted to an object using SeuratWrappers (v.0.3.5), and then trajectory graph learning and pseudotime measurement were performed through reversed graph embedding. The estimation of the root node of the trajectory was based on *Smoc2*.

Velocity analysis. RNA velocities in single cells were calculated with Velocyto (v0.17.15). The arrows that predicted the future state of individual cells were embedded on the Umap plot obtained by Seurat.

GO and KEGG analysis. Gene Ontology (GO) and Kyoto Encyclopedia of Genes and Genomes (KEGG) analyses were conducted using the ClusterProfiler package in R. Genes related to signaling pathway analyses were selected from the differentially expressed genes across groups. Differentially expressed genes were selected with a fold change ≥1.0 and $p < 0.05$.

Bead coating

Recombinant Wnt6 (CSB-EP026140MO, CUSABIO) and Wnt10a (CSB-EP026129MO, CUSABIO) proteins were procured for the preparation of Wnt6-beads and Wnt10a-beads. These proteins were then immobilized onto 2.8 mm carboxylic acid-coated Dynabeads (14305D, Thermo Fisher) following previously established protocols[76,77]. Briefly, the carboxylic acid groups on the Dynabeads were activated through incubation with N-(3-Dimethylaminopropyl)-N′-ethylcarbodiimide (EDC, Sigma) and N-Hydroxysuccinimide (56480−25G, Sigma). Solutions of EDC and NHS at a concentration of 50 mg/mL were prepared in 25 mM cold 2-(N-morpholino) ethanesulfonic acid (M3671-50G, Sigma) buffer at pH 5. The activation process was carried out under constant rotation at room temperature. Post-activation, the beads were captured using a magnet and washed with 25 mM MES buffer. Recombinant Wnt6 and Wnt10a protein (500 ng) was diluted 2.5 mL in MES buffer and incubated with the beads for 1.5 hours under constant rotation at room temperature. Inactivation of beads was achieved through incubation with 20 mM Dithiothreitol (P2325, Life Technologies) for 30 min at 37 °C. Following incubation with DTT, beads were washed with PBS before storage in media containing 10% FBS at 4 °C for up to 2 weeks.

For the preparation of Smoc1-beads, Smoc2-beads and bovine serum albumin (BSA) beads, Affi-Gel agarose beads (100–150 μm diameter; Bio-Rad) were soaked in solutions of 200 ng/μL recombinant Smoc1 proteins (5550-SM-050, R&D Systems), recombinant Smoc2 proteins (6075-SM-050, R&D Systems) and BSA (ST025, Beyotime) at room temperature for 1 hour, respectively. The beads were made and used immediately.

Incisor explant culture

The incisor pulp with epithelium and surrounding dental follicle was dissected from E16.5 wild-type and *Smoc1/2* DKO homozygous embryos in PBS using a dissecting microscope at room temperature, and cultured with a Trowell culture system in vitro[78]. BGjb medium with 10% FBS (Gibco), 2% penicillin/streptomycin (Invitrogen), and 0.1 mg/ml ascorbic acid (Sigma) was used to culture the explant tissue. Wnt6-beads, Wnt10a-beads, and Smoc2-beads were prewashed and soaked in media with 10% FBS at 37 °C for 1 hour. Then the beads were seeded or placed around the apical part of the incisor pulp tissue. The explanted incisors were harvested after 3 days of cultivation and fixed in 4% paraformaldehyde at 4 °C for 1 hour. Samples were washed with PBS and processed with regular dehydration, sectioning, and immunostaining protocols.

MicroCT analysis

The mouse heads were collected and fixed with 4% PFA at 4 °C overnight before being transferred to PBS for MicroCT imaging. Images were captured by using a MicroCT machine (NEMO Micro CT, China) at CIBR with a resolution of 10 μm, and an X-ray source at a voltage 55 kV and current 150 μA.

DPCs culture and treatment

Dental pulp cells (DPCs) were obtained incisor germ from E16.5 wild type mouse embryos and cultured in α-MEM medium consisting of 20% FBS and 100 U/ml penicillin/streptomycin. After two passages, DPCs were used for subsequent experiments. To activate canonical WNT signaling, DPCs were cultured in medium supplemented with 1 μM WNT agonist WAY-262611(WAY, MCE, HY-11035).

Plasmid construct and transfection

The empty vector plasmid was purchased from OriGene (Rockville, MD, USA). The *pCMV6-Smoc1-DDK, pCMV6-Smoc2-DDK, pCMV3-Wnt10a-CFP* and *pCMV3-Gpc6-YFP* plasmids were constructed using Gibson assembly technology. Cells were transfected for overexpression using VIGOROUS Transfection System kit (T001, Vigorous Biotechnology).

siRNA knockdown

To knock down *Gpc6* in DPCs, *Gpc6*-targeting siRNAs were transfected into DPCs according to the manufacturer's instructions (RiboBio, C10511-05). Mouse Gpc6 siRNA (#1: 5′-CTCATGAAGATGCTGTACT-3′, #2: 5′- CACGGAAACTGAAGATTCA-3′) and negative control siRNA were generated by RiboBio (Guangzhou, China).

Western blotting

Cells were harvested and lysed with RIPA lysis buffer (P0013B, Beyotime) plus Protease/Phosphatase Inhibitor Phenylmethylsulfonyl fluoride (ST505, Beyotime) for 30 minutes on ice. Then the supernatant was collected after centrifugation with 12,000 × *g* for 10 minutes. The protein concentrations were quantified through Rapid Gold BCA Protein Assay (Thermo Fisher Scientific, A55861). The proteins were separated by 4-12% SDS-polyacrylamide gel electrophoresis and transferred to polyvinylidene difluoride membranes for blotting. The membranes were blocked in 5% BSA for 1 hour at room temperature, followed by incubation with primary antibodies overnight at 4 °C. After washing three times with PBST, the membranes were incubated with secondary antibodies for 1 hour at room temperature. The proteins were detected by chemiluminescence. The uncropped and unprocessed scans of blots are provided in the Source Data file. The antibodies used in the western blotting were listed as follows: anti-Smoc2 (Santa Cruz Biotechnology, sc376104; 1:500), anti-Smoc1 (Santa Cruz Biotechnology, sc-390448, 1:500), anti-active β-catenin (Cell Signaling Technology, #8814, 1:1000), anti-β-catenin (Cell Signaling Technology, #8480, 1:1000), anti-c-Myc (ABclonal, #A19032, 1:800), anti-CyclinD1 (ABclonal, #A1301, 1:800), anti-LEF1 (ABclonal, #A4473,1:1000), anti-β-Actin (ABclonal, #AC004, 1:1000), anti-Gpc6 (OriGene, TA351222S, 1:800), anti-Wnt10a (Abcam, ab106522, 1:800).

Co-immunoprecipitation (Co-IP)

Cells were collected and lysed with lysis buffer (Cell Signaling Technology) for 30 minutes on ice. After centrifugation at 12,000 × *g* for 10 minutes at 4 °C, the supernatant was collected and incubated with 2.5 μg antibodies overnight at 4 °C followed by incubation with Protein A/G agarose (Santa Cruz) at 4 °C for 2 hours. The anti-Smoc1 Mouse mAb (Santa Cruz Biotechnology, sc-390448), anti-Smoc2 Mouse mAb (Santa Cruz Biotechnology, sc376104), and anti-Gpc6 Rabbit mAb (OriGene, TA351222S) were used for immunoprecipitation of Smoc1, Smoc2, and Gpc6 proteins, respectively. The target protein was collected by centrifugation with 1200 × *g* for 3 min at 4 °C and washed with wash buffer (50 mL PBS with 1 mL 2.5 mM NaF, 500 μL PMSF). The precipitated proteins were separated by SDS-PAGE and detected by immunoblotting using the following antibodies: anti-Smoc1 (OriGene, TA387081M, 1:1000), anti-Smoc2 (OriGene, TA351730, 1:1000), anti-Gpc6 (Thermo Fisher Scientific, MA5-24086, 1:1000), and anti-Wnt10a (Thermo Fisher Scientific, MA5-61312, 1:1000).

Fluorescence resonance energy transfer (FRET)

The interaction between Wnt10a and Gpc6 proteins was monitored by FRET assay. The cells were transfected with donor Wnt10a-CFP plasmid and acceptor Gpc6-YFP plasmid for 24 h. The fluorescence resonance energy transfer was conducted with FRET-Acceptor Bleaching on a Leica SP8 two-photon microscope. FRET efficiency was calculated as: FRETeff = (Dpost − Dpre)/Dpost; Dpost: The intensity before bleached; Dpre: The intensity after bleached.

Statistics & Reproducibility

The number of biological replicates and statistical parameters are indicated in the corresponding figure legends. All experiments, including RNAscope, immunostaining analysis, and pulp culture,e were repeated independently at least three times with similar results. To quantify the percentage of fluorescently labeled cells in the incisor mesenchyme, cells in the region of interest were manually counted using ImageJ (v1.53e). Data are presented as mean ± SEM or mean ± SD, as indicated in the figure legends. Statistical analyses were performed using either GraphPad Prism (version 9.00) or the ggplot2 R package. The chosen level of significance for all statistical tests was $P < 0.05$. No statistical method was used to predetermine sample size. No data were excluded from the analyses. The experiments were not randomized. The investigators were not blinded to allocation during experiments and outcome assessment.

Reporting summary

Further information on research design is available in the Nature Portfolio Reporting Summary linked to this article.

Data availability

The scRNA-seq data generated in this study have been deposited in the GEO database under accession code GSE289364. Source data are provided with this paper.

References

1. Morita, R. et al. Tracing the origin of hair follicle stem cells. *Nature* **594**, 547–552 (2021).
2. Guiu, J. et al. Tracing the origin of adult intestinal stem cells. *Nature* **570**, 107–111 (2019).
3. Berg, D. A. et al. A common embryonic origin of stem cells drives developmental and adult neurogenesis. *Cell* **177**, 654–668.e15 (2019).
4. Fuentealba, L. C. et al. Embryonic origin of postnatal neural stem cells. *Cell* **161**, 1644–1655 (2015).
5. Ghosn, E., Yoshimoto, M., Nakauchi, H., Weissman, I. L. & Herzenberg, L. A. Hematopoietic stem cell-independent hematopoiesis and the origins of innate-like B lymphocytes. *Dev* **146**, 1–15 (2019).
6. Neo, W. H., Lie-A-Ling, M., Fadlullah, M. Z. H. & Lacaud, G. Contributions of Embryonic HSC-independent hematopoiesis to organogenesis and the adult hematopoietic system. *Front. Cell Dev. Biol.* **9**, https://doi.org/10.3389/fcell.2021.631699 (2021).
7. Slack, J. M. W. Origin of stem cells in organogenesis. *Science* **322**, 1498–1501 (2008).
8. Morita, R. & Fujiwara, H. Tracing the developmental origin of tissue stem cells. *Dev. Growth Differ.* **64**, 566–576 (2022).
9. Friedenstein, A. J., Petrakova, K. V., Kurolesova, A. I. & Frolova, G. P. Heterotopic transplants of bone marrow. *Transplantation* **6**, 230–247 (1968).
10. Dellavalle, A. et al. Pericytes resident in postnatal skeletal muscle differentiate into muscle fibres and generate satellite cells. *Nat. Commun.* **2**, 1–11 (2011).
11. Tang, W. et al. White fat progenitor cells reside in the adipose vasculature. *Science* **322**, 583–586 (2008).
12. Knight, M. N. & Hankenson, K. D. Mesenchymal stem cells in bone regeneration. *Adv. Wound Care* **2**, 306–316 (2013).
13. Akiyama, K. et al. Characterization of bone marrow derived mesenchymal stem cells in suspension. *Stem Cell Res. Ther.* **3**, 40 (2012).
14. Miura, M. et al. SHED: Stem cells from human exfoliated deciduous teeth. *Proc. Natl. Acad. Sci. USA.* **100**, 5807–5812 (2003).
15. Takashima, Y. et al. Neuroepithelial cells supply an initial transient wave of MSC differentiation. *Cell* **129**, 1377–1388 (2007).
16. Isern, J. et al. The neural crest is a source of mesenchymal stem cells with specialized hematopoietic stem cell niche function. *Elife* **3**, 1–28 (2014).
17. Dennis, J. E. & Charbord, P. Origin and differentiation of human and murine stroma. *Stem Cells* **20**, 205–214 (2002).
18. Morikawa, S. et al. Development of mesenchymal stem cells partially originate from the neural crest. *Biochem. Biophys. Res. Commun.* **379**, 1114–1119 (2009).
19. Balic, A. & Thesleff, I. *Tissue Interactions Regulating Tooth Development and Renewal. Current Topics in Developmental Biology* vol. 115 (Elsevier Inc., 2015).
20. Krivanek, J., Adameyko, I. & Fried, K. Heterogeneity and developmental connections between cell types inhabiting teeth. *Front. Physiol.* **8**, 1–12 (2017).
21. Shroff, N. P. et al. Proliferation-driven mechanical compression induces signalling centre formation during mammalian organ development. *Nat. Cell Biol.* **26**, 519–529 (2024).
22. Sharir, A. et al. A large pool of actively cycling progenitors orchestrates self-renewal and injury repair of an ectodermal appendage. *Nat. Cell Biol.* **21**, 1102–1112 (2019).
23. Zhao, H. et al. Secretion of shh by a neurovascular bundle niche supports mesenchymal stem cell homeostasis in the adult mouse incisor. *Cell Stem Cell* **14**, 160–173 (2014).
24. Krivanek, J. et al. Dental cell type atlas reveals stem and differentiated cell types in mouse and human teeth. *Nat. Commun.* **11**, 1–18 (2020).
25. Guo, T. et al. Article Vascular architecture regulates mesenchymal stromal cell heterogeneity via P53-PDGF signaling in the mouse incisor Vascular architecture regulates mesenchymal stromal cell heterogeneity via P53-PDGF signaling in the mouse incisor. *Stem Cell* 1–17 https://doi.org/10.1016/j.stem.2024.04.011 (2024).
26. Zhang, M. et al. ARID1B maintains mesenchymal stem cell quiescence via inhibition of BCL11B-mediated non-canonical Activin signaling. *Nat. Commun.* **15**, 1–17 (2024).
27. Jing, J. et al. Reciprocal interaction between mesenchymal stem cells and transit amplifying cells regulates tissue homeostasis. *Elife* **10**, 1–18 (2021).
28. An, Z. et al. A quiescent cell population replenishes mesenchymal stem cells to drive accelerated growth in mouse incisors. *Nat. Commun.* **9**, 1–9 (2018).

29. Chen, S. et al. Runx2+ Niche Cells Maintain Incisor Mesenchymal Tissue Homeostasis through IGF Signaling. *Cell Rep.* **32**, 108007 (2020).
30. Vannahme, C., Gösling, S., Paulsson, M., Maurer, P. & Hartmann, U. Characterization of SMOC-2, a modular extracellular calcium-binding protein. *Biochem. J.* **373**, 805–814 (2003).
31. Kameneva, P. et al. Serotonin limits generation of chromaffin cells during adrenal organ development. *Nat. Commun.* **13**, 1–21 (2022).
32. Seidel, K. et al. Hedgehog signaling regulates the generation of ameloblast progenitors in the continuously growing mouse incisor. *Development* **137**, 3753–3761 (2010).
33. Zhao, H. et al. The suture provides a niche for mesenchymal stem cells of craniofacial bones. *Nat. Cell Biol.* **17**, 386–396 (2015).
34. Jing, J. et al. Spatiotemporal single-cell regulatory atlas reveals neural crest lineage diversification and cellular function during tooth morphogenesis. *Nat. Commun.* **13**, 1–14 (2022).
35. Glover, J. D. et al. *Hierarchical patterning modes orchestrate hair follicle morphogenesis*. *PLoS Biology* **15**, e2002117 (2017).
36. Mu, T. et al. Embryonic liver developmental trajectory revealed by single-cell RNA sequencing in the Foxa2eGFP mouse. *Commun. Biol.* **3**, 1–12 (2020).
37. Wu, X. et al. Spatial multi-omics at subcellular resolution via high-throughput in situ pairwise sequencing. *Nat. Biomed. Eng.* **8**, 872–889 (2024).
38. de Morree, A. & Rando, T. A. Regulation of adult stem cell quiescence and its functions in the maintenance of tissue integrity. *Nat. Rev. Mol. Cell Biol.* **24**, 334–354 (2023).
39. Delgado Lagos, F. et al. Secreted modular calcium-binding protein 1 binds and activates thrombin to account for platelet hyperreactivity in diabetes. *Blood* **137**, 1641–1651 (2021).
40. Takahata, Y. et al. Smoc1 and Smoc2 regulate bone formation as downstream molecules of Runx2. *Commun. Biol.* **4**, 1–11 (2021).
41. Suomalainen, M. & Thesleff, I. Patterns of Wnt pathway activity in the mouse incisor indicate absence of Wnt/β-catenin signaling in the epithelial stem cells. *Dev. Dyn.* **239**, 364–372 (2010).
42. Wang, Y. et al. Single cell atlas of developing mouse dental germs reveals populations of CD24+ and Plac8+ odontogenic cells. *Sci. Bull.* https://doi.org/10.1016/j.scib.2022.03.012 (2022).
43. Alvarez-Rodrigo, I., Willnow, D. & Vincent, J. P. *The logistics of Wnt production and delivery*. *Current Topics in Developmental Biology* vol. 153 (Elsevier Inc., 2023).
44. Rim, E. Y., Clevers, H. & Nusse, R. The Wnt pathway: from signaling mechanisms to synthetic modulators. *Annu. Rev. Biochem.* **91**, 571–598 (2022).
45. McGough, I. J. et al. Glypicans shield the Wnt lipid moiety to enable signalling at a distance. *Nature* **585**, 85–90 (2020).
46. Chai, Y. et al. Fate of the mammalian cranial neural crest during tooth and mandibular morphogenesis. *Development* **127**, 1671–1679 (2000).
47. Le Douarin, N. M., Creuzet, S., Couly, G. & Dupin, E. Neural crest cell plasticity and its limits. *Development* **131**, 4637–4650 (2004).
48. Kalamakis, G. et al. Quiescence modulates stem cell maintenance and regenerative capacity in the aging brain. *Cell* **176**, 1407–1419.e14 (2019).
49. Hsu, Y. C., Li, L. & Fuchs, E. Transit-amplifying cells orchestrate stem cell activity and tissue regeneration. *Cell* **157**, 935–949 (2014).
50. Funk, M. C. et al. Aged intestinal stem cells propagate cell-intrinsic sources of inflammaging in mice. *Dev. Cell* **58**, 2914–2929.e7 (2023).
51. Cho, I. J. et al. Mechanisms, Hallmarks, and implications of stem cell quiescence. *Stem Cell Rep.* **12**, 1190–1200 (2019).
52. van Velthoven, C. T. J. & Rando, T. A. Stem cell quiescence: dynamism, restraint, and cellular idling. *Cell Stem Cell* **24**, 213–225 (2019).
53. Urbain, N. & Cheung, T. H. Stem cell quiescence: The challenging path to activation. *Dev.* **148**, https://doi.org/10.1242/dev.165084 (2021).
54. Furutachi, S. et al. Slowly dividing neural progenitors are an embryonic origin of adult neural stem cells. *Nat. Neurosci.* **18**, 657–665 (2015).
55. Shyer, A. E., Huycke, T. R., Lee, C., Mahadevan, L. & Tabin, C. J. Bending Gradients: How the intestinal stem cell gets its home. *Cell* **161**, 569–580 (2015).
56. Fuchs, E. & Blau, H. M. Tissue stem cells: architects of their niches. *Cell Stem Cell* **27**, 532–556 (2020).
57. Zhao, H., Chai, Y. & Mscs, B. M. Stem Cells in Teeth and Craniofacial Bones. https://doi.org/10.1177/0022034515603972 (2015).
58. Kramann, R. et al. Perivascular Gli1+ progenitors are key contributors to injury-induced organ fibrosis. *Cell Stem Cell* **16**, 51–66 (2015).
59. Jing, D. et al. Response of Gli1+ suture stem cells to mechanical force upon suture expansion. *J. Bone Miner. Res.* **37**, 1307–1320 (2020).
60. Schwartz, A. G., Galatz, L. M. & Thomopoulos, S. Enthesis regeneration: A role for Gli1+ progenitor cells. *Dev* **144**, 1159–1164 (2017).
61. Men, Y. et al. Gli1+ Periodontium stem cells are regulated by osteocytes and occlusal force. *Dev. Cell* **54**, 639–654.e6 (2020).
62. Kaukua, N. et al. Glial origin of mesenchymal stem cells in a tooth model system. *Nature* **513**, 551–554 (2014).
63. Alfawaz, S. et al. Recessive oligodontia linked to a homozygous loss-of-function mutation in the SMOC2 gene. *Arch. Oral. Biol.* **58**, 462–466 (2013).
64. Marchant, T. W. et al. Canine Brachycephaly is associated with a retrotransposon-mediated missplicing of SMOC2. *Curr. Biol.* **27**, 1573–1584.e6 (2017).
65. Jang, B. G., Kim, H. S., Bae, J. M., Kim, W. H. & Kim, H. U. SMOC2, an intestinal stem cell marker, is an independent prognostic marker associated with better survival in colorectal cancers. *Sci. Rep.* 1–14 https://doi.org/10.1038/s41598-020-71643-1 (2020).
66. de Almeida Magalhaes, T. et al. Extracellular carriers control lipid-dependent secretion, delivery, and activity of WNT morphogens. *Dev. Cell* **59**, 244–261.e6 (2024).
67. Mihara, E. et al. Active and water-soluble form of lipidated Wnt protein is maintained by a serum glycoprotein afamin/α-albumin. *Elife* **5**, 1–19 (2016).
68. Norman, M., Vuilleumier, R., Springhorn, A., Gawlik, J. & Pyrowolakis, G. Pentagone internalises glypicans to fine-tune multiple signalling pathways. *Elife* **5**, 1–20 (2016).
69. Thomas, J. T. et al. SMOC can act as both an antagonist and an expander of BMP signaling. *Elife* **6**, 1–22 (2017).
70. Zhao, H., Oka, K., Bringas, P., Kaartinen, V. & Chai, Y. TGF-β type I receptor Alk5 regulates tooth initiation and mandible patterning in a type II receptor-independent manner. *Dev. Biol.* **320**, 19–29 (2008).
71. Birch, H. L. Extracellular matrix and ageing. *Subcell. Biochem.* **90**, 169–190 (2018).
72. Gattazzo, F., Urciuolo, A. & Bonaldo, P. Extracellular matrix: A dynamic microenvironment for stem cell niche. *Biochim. Biophys. Acta - Gen. Subj.* **1840**, 2506–2519 (2014).
73. Thomas, J. T., Chhuy-Hy, L., Andrykovich, K. R. & Moos, M. SMOC binds to pro-EGF, but does not induce Erk Phosphorylation via the EGFR. *PLoS One* **11**, 1–13 (2016).
74. Rainger, J. et al. Loss of the BMP antagonist, SMOC-1, causes Ophthalmo-acromelic (Waardenburg anophthalmia) syndrome in humans and mice. *PLoS Genet.* **7**, e1002114 (2011).
75. Hyun, C. L. et al. The intestinal stem cell marker SMOC2 is an independent prognostic marker associated with better survival in Gastric cancer. *Anticancer Res.* **41**, 3689–3698 (2021).
76. Habib, S. J. et al. A localized Wnt signal orients asymmetric stem cell division in vitro. *Science* **339**, 1445–1448 (2013).

77. Lowndes, M., Junyent, S. & Habib, S. J. Constructing cellular niche properties by localized presentation of Wnt proteins on synthetic surfaces. *Nat. Protoc.* **12**, 1498–1512 (2017).
78. Du, W., Hu, J. K. H., Du, W. & Klein, O. D. Lineage tracing of epithelial cells in developing teeth reveals two strategies for building signaling centers. *J. Biol. Chem.* **292**, 15062–15069 (2017).

Acknowledgements

We thank Mrs. Meng Zhang, Ms. Evelyn Zhao, and Ms. Hayley Zhao for the family support. This study was supported by the startup funding from the Chinese Institute for Brain Research to Hu Zhao, National Natural Science Foundation of China (82370915) to Junjun Jing, and the National Key Research and Development Program of China No. 2022YFA1105800 to Ruili Yang.

Author contributions

H.Z. and J.J. conceived the concept. H.Z., J.J., and R.Y. designed and supervised the study. Z. C. and M.C. performed most of the experiments with equal contribution. Y.W., X.L., Y.H., H.P., J.H., and L.Y. provided technical support. All authors discussed the results and commented on the manuscript text.

Competing interests

The authors declare no competing interests.

Additional information

Supplementary information The online version contains supplementary material available at https://doi.org/10.1038/s41467-025-65705-z.

Correspondence and requests for materials should be addressed to Ruili Yang, Junjun Jing or Hu Zhao.

Peer review information *Nature Communications* thanks Igor Adameyko and the other anonymous reviewer(s) for their contribution to the peer review of this work. A peer review file is available.